PHYSICAL REVIEW D **96,** 014004 (2017)

Heavy quarkonium hybrids: Spectrum, decay, and mixing

Ruben Oncala[1] and Joan Soto[2]

[1]*Nikhef, Science Park 105, 1098 XG Amsterdam, Netherlands*

[2]*Departament de Física Quàntica i Astrofísica and Institut de Ciències del Cosmos, Universitat de Barcelona, Martí i Franquès 1, 08028 Barcelona, Catalonia, Spain*

(Received 20 February 2017; published 10 July 2017)

We present a largely model-independent analysis of the lighter heavy quarkonium hybrids based on the strong coupling regime of potential nonrelativistic QCD. We calculate the spectrum at leading order, including the mixing of static hybrid states. We use potentials that fulfill the required short and long distance theoretical constraints and fit well the available lattice data. We argue that the decay width to the lower lying heavy quarkonia can be reliably estimated in some cases and provide results for a selected set of decays. We also consider the mixing with heavy quarkonium states. We establish the form of the mixing potential at $O(1/m_Q)$, m_Q being the mass of the heavy quarks, and work out its short and long distance constraints. The weak coupling regime of potential nonrelativistic QCD and the effective string theory of QCD are used for that goal. We show that the mixing effects may indeed be important and produce large spin symmetry violations. Most of the isospin zero XYZ states fit well in our spectrum, either as a hybrid or standard quarkonium candidate.

DOI: 10.1103/PhysRevD.96.014004

I. INTRODUCTION

The so-called XYZ states in the charmonium and bottomonium spectrum do not fit in the usual potential model expectations (see Ref. [1] for a recent review). A number of models have been proposed to understand them, ranging from compact tetraquark states to just kinematical enhancements caused by the heavy-light meson pair thresholds. We explore here the possibility that some of these states correspond to heavy quarkonium hybrids in a QCD-based approach. Since charm and bottom masses are much larger than the typical QCD scale $\Lambda_{\rm QCD}$, nonrelativistic QCD (NRQCD) [2,3] can be used for these states. For instance, the spectroscopy of bottomonium hybrids has been studied in lattice NRQCD in Ref. [4], and the production of charmonium hybrids in B decays has been studied in Ref. [5]. Furthermore, if we focus on a region of the spectrum much smaller than $\Lambda_{\rm QCD}$, we should be able to build an effective theory in that region, by integrating out $\Lambda_{\rm QCD}$, in a way similar to the strong coupling regime of potential NRQCD (pNRQCD)[6]. The static limit is relevant for such a construction, and the spectrum in that limit is known from lattice QCD in the case of $n_f = 0$ (no light quarks) [7]. In the Born-Oppenheimer (BO) approximation, each energy level in the static case plays the role of a potential in a Schrödinger equation for the dynamical states built on that static energy level [8]. The static spectrum is displayed in Fig. 1.

The ground state corresponds to the potential for heavy quarkonium states (Σ_g^+), namely, the one that it is usually input in potential models. The higher levels correspond to gluonic excitations and are called hybrid potentials. If we are interested in states of a certain energy, we must in principle take into account all the potentials below that energy, since the states built on different potentials may influence each other through $1/m_Q$ corrections, m_Q being the mass of the heavy quarks ($Q = c, b$). We shall focus here on the lower lying hybrid states built out of Π_u and Σ_u^-. In addition to calculating the spectrum [4,9,10], we will address the question of how they interact with quarkonium, namely, with the states built out of Σ_g^+. The quarkonium states far below the energy of the hybrid states can be integrated out and may contribute to the decay width,

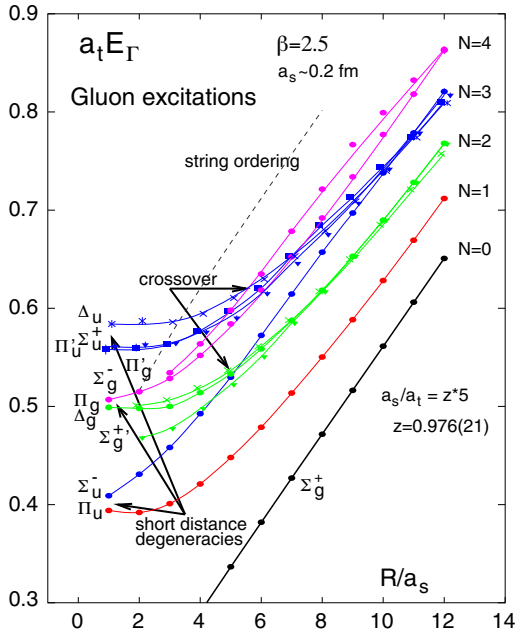

FIG. 1. Energy spectrum in the static limit for $n_f = 0$ [7].

whereas the quarkonium states in the same energy range as hybrid states may mix with them. We will learn that certain hybrid states do not decay to lower lying heavy quarkonium at leading order and that the mixing with quarkonium may induce large spin symmetry violations. These observations will be instrumental in identifying a number of XYZ states as hybrids. In fact, it turns out that most of the XYZ states can eventually be identified with either hybrids or quarkonia in our approach. Preliminary results have been reported in Ref. [11].

The rest of the paper is organized as follows. In Sec. II, we calculate the spectrum of the lower lying hybrid states, ignoring any possible mixing with other states. In Sec. III, we argue that the decay width to lower lying quarkonia can be reliably estimated in some cases and calculate it for a number of states. In Sec. IV, we address the mixing with quarkonium states. We establish the form of the mixing potential at $\mathcal{O}(1/m_Q)$ and derive the short and long distance constraints that it must fulfill using pNRQCD in the weak coupling regime [6,12] and the effective string theory of QCD respectively [13,14]. We explore several interpolations for the mixing potential and recalculate the spectrum. In Secs. V and VI, we compare our results with those of other QCD-based approaches and with the experiment respectively. We also present in the latter the most likely identifications of the XYZ states as hybrids or quarkonia. Section VII contains a discussion of our results. Finally, in Sec. VIII, we present a short summary of the main results and conclude. Appendix A shows our results for quarkonia. Appendix B provides details on how we obtain the two long distance parameters from lattice data. Appendix C sets our conventions for the tensor spherical harmonics. The tables in Appendix D display our results for the full (quarkonium plus hybrid) charmonium and bottomonium spectrum including mixing.

II. SPECTRUM

In the Born-Oppenheimer approximation, the calculation of the hybrid spectrum reduces to solving the Schrödinger equation with a potential $V = V(r, \Lambda_{\rm QCD})$ that has a minimum at $r = r_0 \sim 1/\Lambda_{\rm QCD}$, $r = |\mathbf{r}|$, $\mathbf{r}$ being the distance between the quark and the antiquark. Hence, the energy of the small fluctuations about that minimum is $E \sim \sqrt{\Lambda_{\rm QCD}^3/m_Q} \ll \Lambda_{\rm QCD} \ll m_Q$. Consequently, we are in a situation analogous to the strong coupling regime of pNRQCD in which the scale $\Lambda_{\rm QCD}$ is integrated out. It then makes sense to restrict the study to the lower lying hybrid potentials, Σ_u^- and Π_u, since the gap to the next states is parametrically $O(\Lambda_{\rm QCD})$. Specifically, from Fig. 1, we see that the gap between the minimum of the Π_u potential and the first excited potential that we neglect ($\Sigma_g^{+\prime}$) is about 400 MeV. Hence, for states built out of the Σ_u^- and Π_u potentials about 400 MeV or more above the lowest lying one, mixing effects with the next hybrid multiplet ($\Sigma_g^{+\prime}$, Π_g, Δ_g) may be relevant.

The potentials associated to Σ_u^- and Π_u are degenerated at short distances. In weak coupling pNRQCD [12], this is easily understood as they correspond to different projections with respect to $\mathbf{r}$ of the same operator $\mathrm{tr}(\mathbf{B}(\mathbf{0},t)O(\mathbf{0},\mathbf{r},t))$, where $O(\mathbf{R},\mathbf{r},t)$ is the color octet operator, $\mathbf{B}(\mathbf{R},t)$ the chromemeagnetic field and we have set the center-of-mass coordinate $\mathbf{R} = \mathbf{0}$. These projections have well-defined transformations under the $D_{\infty h}$ group, the group of a diatomic molecule. $\hat{\mathbf{r}}\mathbf{B}$ corresponds to Σ_u^-, and $\mathbf{B} - \hat{\mathbf{r}}(\hat{\mathbf{r}}\mathbf{B})$ corresponds to Π_u [6]. It is then natural to associate to the lower lying hybrids a vectorial wave function $\mathbf{H}(\mathbf{0},\mathbf{r},t)$, such that its projection to $\mathbf{r}$ evolves with $V_{\Sigma_u^-}$ and its projection orthogonal to $\mathbf{r}$ evolves with V_{Π_u}. We then have the following Lagrangian density,

$$\begin{aligned}\mathcal{L} &= \mathrm{tr}(H^{i\dagger}(\delta_{ij} i\partial_0 - h_{Hij})H_j)\\ h_{Hij} &= \left(-\frac{\nabla^2}{m_Q} + V_{\Sigma_u^-}(r)\right)\delta_{ij}\\ &\quad + (\delta_{ij} - \hat{r}_i\hat{r}_j)[V_{\Pi_u}(r) - V_{\Sigma_u^-}(r)],\end{aligned} \tag{1}$$

where $\hat{\mathbf{r}} = \mathbf{r}/|\mathbf{r}|$ and we have ignored the center-of-mass motion. $\mathbf{H} = \mathbf{H}(\mathbf{R},\mathbf{r},t)$ is a matrix in spin space and transforms as $\mathbf{H} \to h_1\mathbf{H}h_2^\dagger$, $h_1,\ h_2 \in SU(2)$ under spin symmetry. h_{Hij} above does not depend on the spin of the quarks, and hence it is invariant under spin symmetry transformations, but it does depend on the total angular momentum of the gluonic degrees of freedom $\mathbf{L}_g$; in this case $L_g = 1$ as is apparent from the vectorial character of $\mathbf{H}$. The symmetry properties of $\mathbf{H}(\mathbf{R},\mathbf{r},t)$ under parity, time reversal, and charge conjugation read as follows,

$$\begin{aligned}P&:\ \mathbf{H}(\mathbf{R},\mathbf{r},t) \to -\mathbf{H}(-\mathbf{R},-\mathbf{r},t)\\ T&:\ \mathbf{H}(\mathbf{R},\mathbf{r},t) \to -\sigma^2\mathbf{H}(\mathbf{R},\mathbf{r},-t)\sigma^2\\ C&:\ \mathbf{H}(\mathbf{R},\mathbf{r},t) \to -\sigma^2\mathbf{H}^T(\mathbf{R},-\mathbf{r},t)\sigma^2,\end{aligned} \tag{2}$$

where σ^2 is the second Pauli matrix. Hence, the P and C associated to a hybrid state with quark-antiquark orbital angular momentum L and quark-antiquark spin S become

$$P = (-1)^{L+1}, \qquad C = (-1)^{L+S+1}. \tag{3}$$

Leaving aside the spin of the quarks, it is convenient to express $\mathbf{H}$ in a basis of eigenfunctions of $\mathbf{J} = \mathbf{L} + \mathbf{L}_g$, where $\mathbf{L}$ is the orbital angular momentum of the quarks. This is achieved using vector spherical harmonics [15],

$$\begin{aligned}\mathbf{H}(\mathbf{r}) = \frac{1}{r}\Bigg(&P_0^+(r)\mathbf{Y}_{00}^{L=1} + \sum_{J=1}^{\infty}\sum_{M=-J}^{J}[P_J^+(r)\mathbf{Y}_{JM}^{L=J+1}\\ &+ P_J^0(r)\mathbf{Y}_{JM}^{L=J} + P_J^-(r)\mathbf{Y}_{JM}^{L=|J-1|}]\Bigg).\end{aligned} \tag{4}$$

Note that $\mathbf{J}$ is a conserved quantity thanks to heavy quark spin symmetry. $\mathbf{Y}^L_{JM} = \mathbf{Y}^L_{JM}(\theta,\phi)$ fulfill

$$\mathbf{J}^2\mathbf{Y}^L_{JM} = J(J+1)\mathbf{Y}^L_{JM}, \qquad \mathbf{L}^2\mathbf{Y}^L_{JM} = L(L+1)\mathbf{Y}^L_{JM},$$
$$\mathbf{L}_g^2\mathbf{Y}^L_{JM} = 2\mathbf{Y}^L_{JM}, \qquad J_3\mathbf{Y}^L_{JM} = M\mathbf{Y}^L_{JM}. \tag{5}$$

The eigenvalue problem then reduces for $J \neq 0$ to

$$\left[-\frac{1}{m_Q}\frac{\partial^2}{\partial r^2} + \begin{pmatrix} \frac{(J-1)J}{m_Q r^2} & 0 \\ 0 & \frac{(J+1)(J+2)}{m_Q r^2} \end{pmatrix} + V_{\Sigma_u^-}(r) + V_q(r)\begin{pmatrix} \frac{J+1}{2J+1} & \frac{\sqrt{(J+1)J}}{2J+1} \\ \frac{\sqrt{(J+1)J}}{2J+1} & \frac{J}{2J+1} \end{pmatrix}\right]\begin{pmatrix} P_J^-(r) \\ P_J^+(r) \end{pmatrix} = E\begin{pmatrix} P_J^-(r) \\ P_J^+(r) \end{pmatrix}$$
$$\left(-\frac{1}{m_Q}\frac{\partial^2}{\partial r^2} + \frac{J(J+1)}{m_Q r^2} + V_{\Pi_u}(r)\right)P_J^0(r) = EP_J^0(r), \tag{6}$$

where $V_q(r) = V_{\Pi_u}(r) - V_{\Sigma_u^-}(r)$, and for $J = 0$ to

$$\left(-\frac{1}{m_Q}\frac{\partial^2}{\partial r^2} + \frac{2}{m_Q r^2} + V_{\Sigma_u^-}(r)\right)P_0^+(r) = EP_0^+(r). \tag{7}$$

The equations above are equivalent to those obtained in Ref. [10]. We approximate $V_{\Pi_u}(r)$ and $V_{\Sigma_u^-}(r)$ by simple functions that have the correct behavior at short and long distances and fit well the lattice results in Fig 1 [7] and Ref. [16]. For $V_{\Sigma_u^-}(r)$, it is enough to take a Cornell-like potential with the correct asymptotic behavior in order to get a good fit to data. We then take

$$V_{\Sigma_u^-}(r) = \frac{\sigma_s}{r} + \kappa_s r + E_s^{Q\bar{Q}}. \tag{8}$$

The correct short and long distance behavior implies $\sigma_s = \sigma_g/8$ and $\kappa_s = \kappa_g$, where σ_g and κ_g are the corresponding parameters appearing in the Cornell potential for heavy quarkonium ($V_{\Sigma_g^+}(r)$); see Appendix A. We then have

$$\sigma_s = 0.061, \qquad \kappa_s = 0.187\ \text{GeV}^2. \tag{9}$$

The constant $E_s^{Q\bar{Q}}$ becomes then the only free parameter, which can be linked to the corresponding parameter for the heavy quarkonium case, $E_g^{Q\bar{Q}}$, through the lattice data of Ref. [7]. Finally, $E_g^{Q\bar{Q}}$ is obtained in Appendix A by fitting the heavy quarkonium spectrum. We get

$$E_s^{c\bar{c}} = 0.559\ \text{GeV}, \qquad E_s^{b\bar{b}} = 0.573\ \text{GeV}. \tag{10}$$

For $V_{\Pi_u}(r)$, a Cornell-like form does not fit lattice data well at intermediate distances. Hence, we take a slightly more complicated form for it,

$$V_{\Pi_u}(r) = \frac{\sigma_p}{r}\left(\frac{1 + b_1 r + b_2 r^2}{1 + a_1 r + a_2 r^2}\right) + \kappa_p r + E_p^{Q\bar{Q}}. \tag{11}$$

At short distances, this potential must coincide with $V_{\Sigma_u^-}(r)$ up to terms that vanish when $r \to 0$ [6]. This implies $\sigma_p = \sigma_s$ and $E_p^{Q\bar{Q}} - E_s^{Q\bar{Q}} + \sigma_p(b_1 - a_1) = 0$. At long distances, it must be consistent with the effective string theory of QCD [14],

$$E_N(r \to \infty) = \kappa r + \left(\pi N - \frac{(D-2)\pi}{24}\right)\frac{1}{r} + O(1/r^2), \tag{12}$$

where D is the space-time dimension and N labels the energy spectrum of the string. The leading term of this formula implies $\kappa_p = \kappa_s = \kappa$. The next-to-leading term provides the extra constraint,

$$2\pi - \sigma_s + \frac{\sigma_p b_2}{a_2} = 0, \tag{13}$$

which follows from Fig. 1 [7]. Indeed, those data show the nontrivial fact that the $V_{\Pi_u}(r)$ and $V_{\Sigma_u^-}(r)$ potentials at long distances correspond to the $N = 1$ and $N = 3$ string energy levels respectively. Putting together all the constraints above allows us to solve a_1, b_1, and b_2 as a function of known parameters and $E_p^{Q\bar{Q}}$ and a_2, which are fitted to lattice data. We obtain

$$\sigma_p = 0.061, \qquad \kappa_p = 0.187\ \text{GeV}^2$$
$$b_1 = 0.06964\ \text{GeV}, \qquad b_2 = -1.45934\ \text{GeV}^2$$
$$a_1 = -0.06733\ \text{GeV}, \qquad a_2 = 0.01433\ \text{GeV}^2$$
$$E_p^{c\bar{c}} = 0.551\ \text{GeV}, \qquad E_p^{b\bar{b}} = 0.565\ \text{GeV}. \tag{14}$$

The central value of lattice data and the outcome of the fits above are shown in Fig. 2, together with the potential for quarkonium $V_{\Sigma_g^+}$ discussed in the Appendix A.

Using the potentials above as an input, we solve (6) and (7) and obtain the results displayed in Tables I and II in terms of $M_{Q\bar{Q}g} = 2m_Q + E$. Details on the code used can be found in Ref. [17]. We have also displayed the results in Figs. 3 and 4, where we have included the errors discussed at the end of Sec. IV C.

III. DECAY

Since we are interested in the lower lying hybrid states, it is enough for us to consider an effective theory for energy fluctuations much smaller than Λ_{QCD} around those states. The energy gap to the lower lying quarkonium states is greater than Λ_{QCD}. Hence, those states can be integrated out, which will give rise to an imaginary potential ΔV, which in turn will produce the semi-inclusive decay width

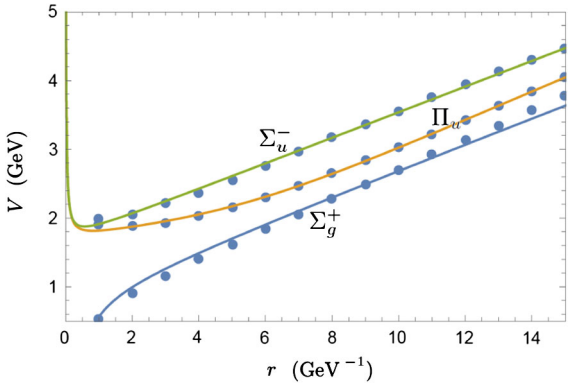

FIG. 2. Our fits to the lattice results of Ref. [7] for the three lower lying BO potentials $V_{\Sigma_g^+}$, V_{Π_u}, and $V_{\Sigma_u^-}$.

for a hybrid state to decay into any quarkonium state, $\Gamma_{H_m\to S} = -2\langle H_m|\mathrm{Im}\Delta V|H_m\rangle$. This is much in the same way as integrating out hard gluons in QCD produces operators with imaginary matching coefficients in NRQCD [3], which give rise to the total decay width of a given quarkonium state to light degrees of freedom. Furthermore, if we assume that the energy gap to a given quarkonium state S_n, ΔE_{mn}, fulfills $\Delta E_{mn} \gg \Lambda_{\rm QCD}$ and that the process is short distance dominated, the integration for that state can be done using the weak coupling regime of pNRQCD [6,12],

$$\begin{aligned}\mathcal{L}_{\rm pNRQCD} &= \mathrm{Tr}\{\mathrm{S}^\dagger(i\partial_0 - h_s)\mathrm{S} + \mathrm{O}^\dagger(iD_0 - h_o)\mathrm{O}\} \\ &+ \mathrm{Tr}\left\{\mathrm{O}^\dagger \mathbf{r}\cdot g\mathbf{E}\mathrm{S} + \mathrm{H.c.} + \frac{\mathrm{O}^\dagger \mathbf{r}\cdot g\mathbf{E}\mathrm{O}}{2} + \frac{\mathrm{O}^\dagger \mathrm{O}\mathbf{r}\cdot g\mathbf{E}}{2}\right\} \\ &+ \cdots . \end{aligned} \tag{15}$$

The singlet field S encodes the quarkonium states, whereas the octet field O encodes the heavy quark content of the hybrid states, h_s and h_o are Hamiltonians containing the respective Coulomb-type potentials, and $\mathbf{E} = \mathbf{E}(\mathbf{R}, t)$ is the chromoelectric field (see Ref. [19] for details). The leading contribution corresponds to the diagram in Fig. 5. We obtain

$$\mathrm{Im}\Delta V = -\frac{2}{3}\frac{\alpha_s T_F}{N_c}\sum_n r^i|S_n\rangle\langle S_n|r^i(i\partial_t - E_n)^3, \tag{16}$$

$T_F = 1/2$, $N_c = 3$, and $\alpha_s = g^2/4\pi$ is the QCD strong coupling constant. E_n is the energy of the nth quarkonium state, S_n.

From the expression above, we identify

$$\Gamma(H_m \to S_n) = \frac{4}{3}\frac{\alpha_s T_F}{N_c}\langle H_m|r^i|S_n\rangle\langle S_n|r^i|H_m\rangle\Delta E_{mn}^3. \tag{17}$$

$\Delta E_{mn} = E_m - E_n$, E_m being the energy of the hybrid state. At this order, the decays respect heavy quark spin symmetry, and hence the spin of the heavy quarks must be the same in the initial hybrid state and in the final quarkonium state. In addition, a selection rule derived from this formula is that hybrid states with $L = J$ do not decay to lower lying quarkonium. This selection rule will be instrumental later on to select hybrid candidates among competing XYZ states. For the allowed decays, the numerical values of the

TABLE I. Charmonium (S) and hybrid charmonium (P^{+-0}) energy spectrum computed with $m_c = 1.47$ GeV. Masses are in MeV. States which only differ by the heavy quark spin ($S = 0, 1$) are degenerated. N is the principal quantum number, L is the orbital angular momentum of the heavy quarks, J is L plus the total angular momentum of the gluons, S is the spin of the heavy quarks, and $\mathcal{J}$ is the total angular momentum. For the quarkonium, J coincides with L, and it is not displayed. The last column shows the relevant potentials for each state. The $(s/d)_1$, p_1, p_0, $(p/f)_2$, and d_2 states are named H_1, H_2, H_3, H_4, and H_5 respectively in Ref. [10].

NL_J	w-f	$M_{c\bar{c}}$	$M_{c\bar{c}g}$	$S=0$ $\mathcal{J}^{PC}$	$S=1$ $\mathcal{J}^{PC}$	Λ_η^ϵ
$1s$	S	3068		0^{-+}	1^{--}	Σ_g^+
$2s$	S	3678		0^{-+}	1^{--}	Σ_g^+
$3s$	S	4131		0^{-+}	1^{--}	Σ_g^+
$1p_0$	P^+		4486	0^{++}	1^{+-}	Σ_u^-
$4s$	S	4512		0^{-+}	1^{--}	Σ_g^+
$2p_0$	P^+		4920	0^{++}	1^{+-}	Σ_u^-
$3p_0$	P^+		5299	0^{++}	1^{+-}	Σ_u^-
$4p_0$	P^+		5642	0^{++}	1^{+-}	Σ_u^-
$1p$	S	3494		1^{+-}	$(0,1,2)^{++}$	Σ_g^+
$2p$	S	3968		1^{+-}	$(0,1,2)^{++}$	Σ_g^+
$1(s/d)_1$	P^{+-}		4011	1^{--}	$(0,1,2)^{-+}$	$\Pi_u\Sigma_u^-$
$1p_1$	P^0		4145	1^{++}	$(0,1,2)^{+-}$	Π_u
$2(s/d)_1$	P^{+-}		4355	1^{--}	$(0,1,2)^{-+}$	$\Pi_u\Sigma_u^-$
$3p$	S	4369		1^{+-}	$(0,1,2)^{++}$	Σ_g^+
$2p_1$	P^0		4511	1^{++}	$(0,1,2)^{+-}$	Π_u
$3(s/d)_1$	P^{+-}		4692	1^{--}	$(0,1,2)^{-+}$	$\Pi_u\Sigma_u^-$
$4(s/d)_1$	P^{+-}		4718	1^{--}	$(0,1,2)^{-+}$	$\Pi_u\Sigma_u^-$
$4p$	S	4727		1^{+-}	$(0,1,2)^{++}$	Σ_g^+
$3p_1$	P^0		4863	1^{++}	$(0,1,2)^{+-}$	Π_u
$5(s/d)_1$	P^{+-}		5043	1^{--}	$(0,1,2)^{-+}$	$\Pi_u\Sigma_u^-$
$5p$	S	5055		1^{+-}	$(0,1,2)^{++}$	Σ_g^+
$1d$	S	3793		2^{-+}	$(1,2,3)^{--}$	Σ_g^+
$2d$	S	4210		2^{-+}	$(1,2,3)^{--}$	Σ_g^+
$1(p/f)_2$	P^{+-}		4231	2^{++}	$(1,2,3)^{+-}$	$\Pi_u\Sigma_u^-$
$1d_2$	P^0		4334	2^{--}	$(1,2,3)^{-+}$	Π_u
$2(p/f)_2$	P^{+-}		4563	2^{++}	$(1,2,3)^{+-}$	$\Pi_u\Sigma_u^-$
$3d$	S	4579		2^{-+}	$(1,2,3)^{--}$	Σ_g^+
$2d_2$	P^0		4693	2^{--}	$(1,2,3)^{-+}$	Π_u
$3(p/f)_2$	P^{+-}		4886	2^{++}	$(1,2,3)^{+-}$	$\Pi_u\Sigma_u^-$
$4d$	S	4916		2^{-+}	$(1,2,3)^{--}$	Σ_g^+
$4(p/f)_2$	P^{+-}		4923	2^{++}	$(1,2,3)^{+-}$	$\Pi_u\Sigma_u^-$
$3d_2$	P^0		5036	2^{--}	$(1,2,3)^{-+}$	Π_u

TABLE II. Bottomonium (S) and hybrid bottomonium (P^{+-0}) energy spectrum computed with $m_b = 4.88$ GeV. Masses are in MeV. States which only differ by the heavy quark spin ($S = 0, 1$) are degenerated. N is the principal quantum number, L is the orbital angular momentum of the heavy quarks, J is L plus the total angular momentum of the gluons, S is the spin of the heavy quarks, and $\mathcal{J}$ is the total angular momentum. For the quarkonium, J coincides with L, and it is not displayed. The last column shows the relevant potentials for each state. The $(s/d)_1$, p_1, p_0, $(p/f)_2$, and d_2 states are named H_1, H_2, H_3, H_4, and H_5 respectively in Ref. [10].

NL_J	w-f	$M_{b\bar{b}}$	$M_{b\bar{b}g}$	$S{=}0$ $\mathcal{J}^{PC}$	$S{=}1$ $\mathcal{J}^{PC}$	Λ_η^ϵ
$1s$	S	9442		0^{-+}	1^{--}	Σ_g^+
$2s$	S	10 009		0^{-+}	1^{--}	Σ_g^+
$3s$	S	10 356		0^{-+}	1^{--}	Σ_g^+
$4s$	S	10 638		0^{-+}	1^{--}	Σ_g^+
$1p_0$	P^+		11 011	0^{++}	1^{+-}	Σ_u^-
$2p_0$	P^+		11 299	0^{++}	1^{+-}	Σ_u^-
$3p_0$	P^+		11 551	0^{++}	1^{+-}	Σ_u^-
$4p_0$	P^+		11 779	0^{++}	1^{+-}	Σ_u^-
$1p$	S	9908		1^{+-}	$(0,1,2)^{++}$	Σ_g^+
$2p$	S	10 265		1^{+-}	$(0,1,2)^{++}$	Σ_g^+
$3p$	S	10 553		1^{+-}	$(0,1,2)^{++}$	Σ_g^+
$1(s/d)_1$	P^{+-}		10 690	1^{--}	$(0,1,2)^{-+}$	$\Pi_u\Sigma_u^-$
$1p_1$	P^0		10 761	1^{++}	$(0,1,2)^{+-}$	Π_u
$4p$	S	10 806		1^{+-}	$(0,1,2)^{++}$	Σ_g^+
$2(s/d)_1$	P^{+-}		10 885	1^{--}	$(0,1,2)^{-+}$	$\Pi_u\Sigma_u^-$
$2p_1$	P^0		10 970	1^{++}	$(0,1,2)^{+-}$	Π_u
$5p$	S	11 035		1^{+-}	$(0,1,2)^{++}$	Σ_g^+
$3(s/d)_1$	P^{+-}		11 084	1^{--}	$(0,1,2)^{-+}$	$\Pi_u\Sigma_u^-$
$4(s/d)_1$	P^{+-}		11 156	1^{--}	$(0,1,2)^{-+}$	$\Pi_u\Sigma_u^-$
$3p_1$	P^0		11 175	1^{++}	$(0,1,2)^{+-}$	Π_u
$6p$	S	11 247		1^{+-}	$(0,1,2)^{++}$	Σ_g^+
$5(s/d)_1$	P^{+-}		11 284	1^{--}	$(0,1,2)^{-+}$	$\Pi_u\Sigma_u^-$
$1d$	S	10 155		2^{-+}	$(1,2,3)^{--}$	Σ_g^+
$2d$	S	10 454		2^{-+}	$(1,2,3)^{--}$	Σ_g^+
$3d$	S	10 712		2^{-+}	$(1,2,3)^{--}$	Σ_g^+
$1(p/f)_2$	P^{+-}		10 819	2^{++}	$(1,2,3)^{+-}$	$\Pi_u\Sigma_u^-$
$1d_2$	P^0		10 870	2^{--}	$(1,2,3)^{-+}$	Π_u
$4d$	S	10 947		2^{-+}	$(1,2,3)^{--}$	Σ_g^+
$2(p/f)_2$	P^{+-}		11 005	2^{++}	$(1,2,3)^{+-}$	$\Pi_u\Sigma_u^-$
$2d_2$	P^0		11 074	2^{--}	$(1,2,3)^{-+}$	Π_u
$5d$	S	11 163		2^{-+}	$(1,2,3)^{--}$	Σ_g^+
$3(p/f)_2$	P^{+-}		11 197	2^{++}	$(1,2,3)^{+-}$	$\Pi_u\Sigma_u^-$
$3d_2$	P^0		11 275	2^{--}	$(1,2,3)^{-+}$	Π_u
$4(p/f)_2$	P^{+-}		11 291	2^{++}	$(1,2,3)^{+-}$	$\Pi_u\Sigma_u^-$

decay widths are given in Table III. We have only displayed numbers that can be reliably estimated, namely, that ΔE_{mn} is large enough and that $\langle H_m|r^i|S_n\rangle$ is small enough so that the weak coupling regime of pNRQCD is sensible; see the

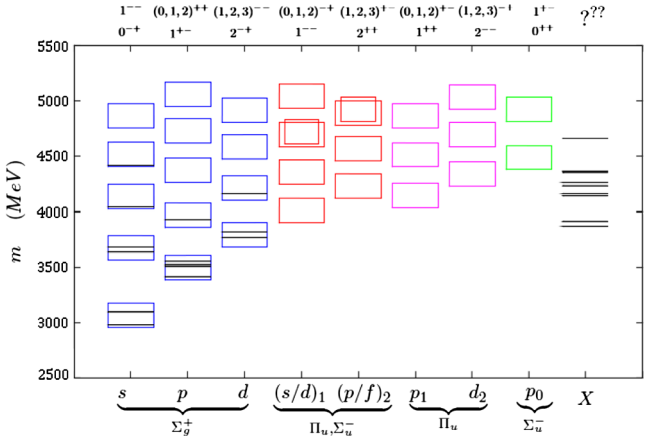

FIG. 3. Charmonium spectrum in Table I. The height of the boxes corresponds to the error estimated at the end of Sec. IV C. The states identified as quarkonium in the Particle Data Group (PDG) [18] are displayed in the corresponding column, whereas the states labeled as X in the PDG [18] are displayed in a separated column. The box assignment of the latter is discussed in Sec. VI.

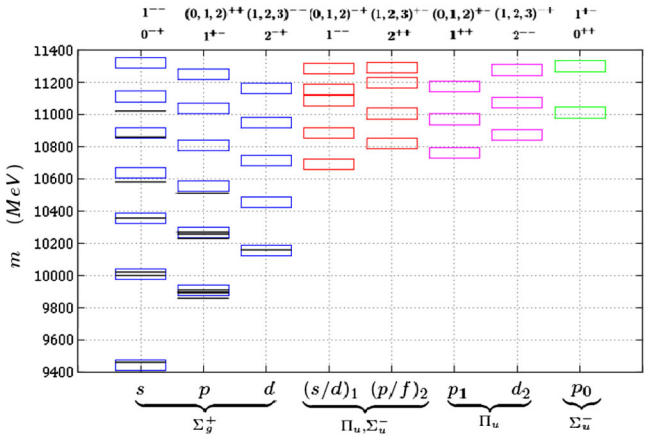

FIG. 4. Bottomonium spectrum in Table II. The height of the boxes corresponds to the error estimated at the end of Sec. IV C. The states identified as quarkonium in the PDG [18] are displayed in the corresponding column.

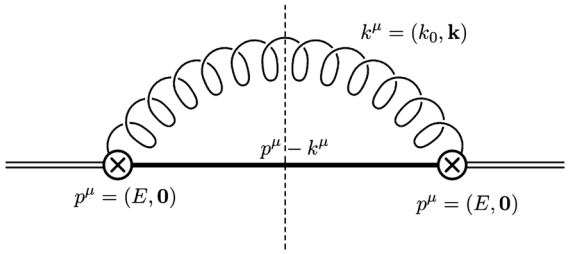

FIG. 5. The octet field self-energy diagram in weak coupling pNRQCD [19]. The double line represents the octet propagator, while single lines represent the singlet propagator. The curly line stands for the gluon propagator, and the crossed circles stand for chromoelectric dipole vertices. The expectator gluons that make up the physical state together with the octet field are not displayed.

TABLE III. Decay widths for hybrid charmonium (above) and bottomonium (below) to lower lying charmonia and bottomonia respectively. $m = NL_J$, $n = N'L'$, $\Delta E \equiv \Delta E_{mn}$, and Γ are in MeV, and $\langle r\rangle_{mn}$ is in GeV^{-1}. $\alpha_s(\Delta E)$ is the one-loop running coupling constant at the scale ΔE. We only display results for which $\Delta E > 800$ MeV and $|\Delta E\langle r\rangle_{mn}| < 0.7$. The error (in brackets) includes higher orders in α_s and in the multipole expansion as well as the average of the linear term in the Cornell potential in order to account for the difference between weak and strong coupling regimes.

$NL_J \to N'L'$	ΔE	$\langle r\rangle_{mn}$	$\lvert\Delta E\langle r\rangle_{mn}\rvert$	$\alpha_s(\Delta E)$	Γ (MeV)
$1p_0 \to 2s$	808	0.40	0.32	0.41	7.5(7.4)
$2(s/d)_1 \to 1p$	861	0.63	0.54	0.39	22(19)
$4(s/d)_1 \to 1p$	1224	0.42	0.51	0.33	23(15)
$1p_0 \to 1s$	1569	−0.42	0.65	0.29	44(23)
$1p_0 \to 2s$	1002	0.43	0.43	0.36	15(9)
$2p_0 \to 2s$	1290	−0.14	0.18	0,32	2.9(1.3)
$2p_0 \to 3s$	943	0.46	0.44	0.37	15(12)
$4p_0 \to 1s$	2337	0.27	0.63	0.25	53(25)
$4p_0 \to 2s$	1770	0.23	0.40	0.28	18(7)
$4p_0 \to 3s$	1423	0.19	0.28	0.31	7.4(4.1)
$2(s/d)_1 \to 1p$	977	0.47	0.46	0.37	17(8)
$3(s/d)_1 \to 1p$	1176	0.49	0.58	0.33	29(14)
$3(s/d)_1 \to 2p$	818	0.32	0.26	0.40	5(3)
$4(s/d)_1 \to 2p$	891	−0.74	0.66	0.39	33(25)
$5(s/d)_1 \to 1p$	1376	−0.31	0.43	0.31	18(7)
$5(s/d)_1 \to 2p$	1018	−0.41	0.42	0.36	14(8)

table caption for details. We have taken the energies and wave functions for quarkonium and for hybrids from Appendix A and from the previous section respectively. The errors account for the fact that the quarkonium spectrum in (16) is meant to be calculated in the weak coupling regime (Coulomb-type bound states), whereas we actually use in (17) the one in the strong coupling regime.

Model-independent results for hybrid decays in the Born-Oppenheimer approximation have been obtained before in Ref. [20]. In that reference, selection rules, based on the symmetries of the static limit, are obtained for a two-body decay of a hybrid to a quarkonium plus a light meson, which constrains the possible quantum numbers of the latter. Our results are obtained under different assumptions and may be regarded as complementary to those of Ref. [20]. First of all, our results hold beyond the static limit (e.g. $\Pi_u - \Sigma_u^-$ mixing is taken into account). Second, they are concerned with semi-inclusive decays, namely, decays to quarkonium plus any state composed of light hadrons, rather than two-body decays. And third, they are based on the additional dynamical assumption that the decay process is short distance dominated. This assumption must be verified for each particular decay and does not always hold. In the cases it does, we are able to put forward not only constraints on quantum numbers (e.g. L must be different from J for a hybrid to decay to quarkonium) but also numerical estimates for the decay widths.

IV. MIXING

So far, we have not taken into account the possible mixing of hybrid states with other states that are known to exist in the same energy range, like quarkonium or heavy-light meson pairs, which may distort the spectrum and the decay properties. We shall focus here on the effects in the spectrum of the mixing with the quarkonium, basically because they are amenable to a systematic treatment. In the static limit, the quarkonium (the lowest potential in Fig. 1, Σ_g^+) and heavy hybrids (the remaining potentials in Fig. 1) do not mix by construction (they are built as orthogonal states). Hence, the mixing must be due to $1/m_Q$ corrections to the Born-Oppenheimer approximation.[1] A way to systematically compute $1/m_Q$ corrections for quarkonium was established in Refs. [21,22] for the strong coupling regime of pNRQCD, following earlier work in the literature [23]. We show below how the formalism in Ref. [21] can also be used to calculate the mixing potentials. We may generally consider an effective theory for energy fluctuations E around a hybrid state, such that $E \ll \Lambda_{\mathrm{QCD}}$. If there is a heavy quarkonium state close to that energy, we may expect it to modify the value of the energy E. This effective theory reads

$$\mathcal{L}_{H+S} = \mathrm{tr}(S^\dagger[i\partial_0 - h_s]S) + \mathrm{tr}(H^{i\dagger}[i\delta_{ij}\partial_0 - h_{Hij}]H^j) + \mathrm{tr}(S^\dagger V_S^{ij}\{\sigma^i, H^j\} + \mathrm{H.c.}). \quad (18)$$

The traces are over spin indices, and

$$V_S^{ij} = V_S^{ij}(\mathbf{r}) = \delta^{ij}V_S^\Pi(r) + \hat{r}^i\hat{r}^j(V_S^\Sigma(r) - V_S^\Pi(r)) \quad (19)$$

is the mixing potential, $h_s = -\frac{\boldsymbol{\nabla}^2}{m_Q} + V_{\Sigma_g^+}(r)$, and h_{Hij} is defined in (1). $S = S(\mathbf{R}, \mathbf{r}, t)$ transforms like $\mathbf{H}$ under heavy quark spin symmetry and as follows under the discrete symmetries [19]:

$$\begin{aligned} P&:\ S(\mathbf{R},\mathbf{r},t) \to -S(-\mathbf{R},-\mathbf{r},t) \\ T&:\ S(\mathbf{R},\mathbf{r},t) \to \sigma^2 S(\mathbf{R},\mathbf{r},-t)\sigma^2 \\ C&:\ S(\mathbf{R},\mathbf{r},t) \to \sigma^2 S^T(\mathbf{R},-\mathbf{r},t)\sigma^2. \end{aligned} \quad (20)$$

The transformations above together with those in (3) dictate the form of the last (mixing) term in (18). The form of $V_S^{ij}(\mathbf{r})$ then follows from the symmetries of the static limit (see for instance Ref. [19]). Notice that in (18) we only include the $1/m_Q$ corrections relevant to the mixing. There are also $1/m_Q$ corrections to h_s [21] and to h_{Hij}, briefly discussed in Sec. VII, that we do not consider. For systems with the quark and antiquark of different flavor, two more terms, which vanish in the equal mass limit, are possible,

[1] In the weak coupling regime of pNRQCD, some $\mathbf{p}/m_Q$ contributions can be reshuffled into $\mathbf{r}i\partial_0$, which have the same size, by local field redefinitions [6,12,19]. This is why singlet-octet transition terms appear in (15) with no apparent $1/m_Q$ suppression.

$$\delta\mathcal{L}_{H+S} = \mathrm{tr}(S^\dagger V_S'^{ij}[\sigma^i, H^j]) + \mathrm{tr}(S^\dagger V_L^{ij} L^i H^j) + \mathrm{H.c.}, \quad (21)$$

where L^i is the angular momentum operator.

A. Matching to NRQCD at $\mathcal{O}(1/m_Q)$

The NRQCD operators that create states at time t with the same quantum numbers as S and $\mathbf{H}$ in the static limit read

$$\begin{aligned}\hat{O}^\dagger(\mathbf{r},\mathbf{R},t) &\equiv \psi^\dagger\left(\frac{\mathbf{r}}{2},t\right) W\left(\frac{\mathbf{r}}{2},-\frac{\mathbf{r}}{2};t\right)\chi\left(-\frac{\mathbf{r}}{2},t\right)\\ &= Z_S^{1/2}(r) S^\dagger(\mathbf{r},\mathbf{R},t)\\ \hat{O}_B^{\dagger i}(\mathbf{r},\mathbf{R},t) &\equiv \psi^\dagger\left(\frac{\mathbf{r}}{2},t\right) W\left(\frac{\mathbf{r}}{2},\mathbf{R};t\right) B^i(\mathbf{R};t) W\left(\mathbf{R},-\frac{\mathbf{r}}{2};t\right)\\ &\quad\times\chi\left(-\frac{\mathbf{r}}{2},t\right) = (Z_H^{1/2})^{ij}(\mathbf{r}) H^{\dagger j}(\mathbf{r},\mathbf{R},t), \quad (22)\end{aligned}$$

where $W(\mathbf{r},\mathbf{r}';t)$ are straight Wilson lines joining the points $\mathbf{r}$ and $\mathbf{r}'$ at a fixed time t, and

$$(Z_H^{1/2})^{ij}(\mathbf{r}) = Z_\Sigma^{1/2}(r)\hat{r}^i\hat{r}^j + Z_\Pi^{1/2}(r)(\delta^{ij} - \hat{r}^i\hat{r}^j). \quad (23)$$

In the static limit, we have

$$\begin{aligned}&\langle 0|T\{\hat{O}^\dagger(\mathbf{r}',\mathbf{R}',T/2)\hat{O}(\mathbf{r},\mathbf{R},-T/2)\}|0\rangle\\ &\quad= \langle 1\rangle_\square \delta(\mathbf{r}'-\mathbf{r})\delta(\mathbf{R}'-\mathbf{R})\\ &\langle 0|T\{\hat{O}_B^{\dagger i}(\mathbf{r}',\mathbf{R}',T/2)\hat{O}_B^j(\mathbf{r},\mathbf{R},-T/2)\}|0\rangle\\ &\quad= \langle B^i(\mathbf{R}',T/2)B^j(\mathbf{R};-T/2)\rangle_\square \delta(\mathbf{r}'-\mathbf{r})\delta(\mathbf{R}'-\mathbf{R}),\end{aligned} \quad (24)$$

where $\langle\ldots\rangle_\square$ means insertions in the square Wilson loop going from $-T/2$ to $T/2$ with spatial boundaries at $\mathbf{R}\pm\mathbf{r}/2$. In particular, $\langle 1\rangle_\square$ is the Wilson loop itself. The matching calculation at $\mathcal{O}(1)$ leads to

$$\begin{aligned}&\langle 1\rangle_\square = Z_S e^{-iTV_{\Sigma_g^+}(r)}\\ &\langle B^i(\mathbf{R},T/2)B^j(\mathbf{R};-T/2)\rangle_\square\\ &\quad= \hat{r}^i\hat{r}^j Z_\Sigma e^{-iTV_{\Sigma_u^-}(r)} + (\delta^{ij}-\hat{r}^i\hat{r}^j) Z_\Pi e^{-iTV_{\Pi_u}(r)}.\end{aligned} \quad (25)$$

Hence, $V_{\Sigma_u^-}(r)$ and $V_{\Pi_u}(r)$ can be obtained from large T behavior of certain operator insertions in the Wilson loop and have long been known from lattice calculations [7,8,24].

The NRQCD Lagrangian density at $\mathcal{O}(1/m_Q)$ reads

$$\begin{aligned}\mathcal{L}_{\mathrm{NRQCD}} &= \psi^\dagger\left[iD_0 + \frac{\mathbf{D}^2}{2m_Q} + gc_F\frac{\boldsymbol{\sigma}\mathbf{B}}{2m_Q}\right]\psi\\ &\quad+\chi^\dagger\left[iD_0 - \frac{\mathbf{D}^2}{2m_Q} - gc_F\frac{\boldsymbol{\sigma}\mathbf{B}}{2m_Q}\right]\chi,\end{aligned} \quad (26)$$

where c_F is a matching coefficient that will eventually be approximated by its tree level value $c_F = 1$. Since the Lagrangian above contains a spin-dependent term, we expect the leading contribution to V_S^{ij} to appear at $\mathcal{O}(1/m_Q)$. We can easily get it by matching the following correlation function at $\mathcal{O}(1/m_Q)$,

$$\begin{aligned}&\langle 0|T\{\hat{O}(\mathbf{r}',\mathbf{R}',T/2)\hat{O}_B^{\dagger i}(\mathbf{r},\mathbf{R},-T/2)\}|0\rangle\\ &\quad= Z_S^{1/2}(Z_H^{1/2})^{ij}(\mathbf{r})\langle 0|T\{S(\mathbf{r}',\mathbf{R}',T/2)H^{\dagger j}(\mathbf{r},\mathbf{R},-T/2)\}|0\rangle,\end{aligned} \quad (27)$$

and focusing on the spin-dependent terms. The lhs is calculated using first order in perturbation theory in $1/m_Q$ in NRQCD (26). The rhs is calculated again at first order in perturbation theory in $1/m_Q$ from (18) [recall that V_S^{ij} is treated as $\mathcal{O}(1/m_Q)$]. Taking into account (19), we obtain

$$\begin{aligned}&\frac{\frac{gc_F}{2m_Q}\int_{-T/2}^{T/2} dt\langle\hat{\mathbf{r}}\mathbf{B}(\frac{\mathbf{r}}{2},t)\hat{\mathbf{r}}\mathbf{B}(\mathbf{0},-T/2)\rangle_\square}{\langle 1\rangle_\square^{1/2}\langle\hat{\mathbf{r}}\mathbf{B}(\mathbf{0},T/2)\hat{\mathbf{r}}\mathbf{B}(\mathbf{0},-T/2)\rangle_\square^{1/2}}\\ &\quad= 2V_S^\Sigma\frac{\sin\left((V_{\Sigma_u^-}-V_{\Sigma_g^+})T/2\right)}{V_{\Sigma_u^-}-V_{\Sigma_g^+}}\end{aligned} \quad (28)$$

$$\begin{aligned}&\frac{\frac{gc_F}{2m_Q}\int_{-T/2}^{T/2} dt}{\langle 1\rangle_\square^{1/2}}\\ &\times\frac{\langle\mathbf{B}(\frac{\mathbf{r}}{2},t)\mathbf{B}(\mathbf{0},-T/2) - \hat{\mathbf{r}}\mathbf{B}(\frac{\mathbf{r}}{2},t)\hat{\mathbf{r}}\mathbf{B}(\mathbf{0},-T/2)\rangle_\square}{\langle\mathbf{B}(\mathbf{0},T/2)\mathbf{B}(\mathbf{0},-T/2) - \hat{\mathbf{r}}\mathbf{B}(\mathbf{0},T/2)\hat{\mathbf{r}}\mathbf{B}(\mathbf{0},-T/2)\rangle_\square^{1/2}}\\ &= 2\sqrt{2}V_S^\Pi\frac{\sin\left((V_{\Pi_u}-V_{\Sigma_g^+})T/2\right)}{V_{\Pi_u}-V_{\Sigma_g^+}}.\end{aligned} \quad (29)$$

Notice that the Euclidean version of the objects on the lhs can be easily calculated on the lattice. At large T, V_S^Σ and V_S^Π can be then extracted by matching the data to the Euclidean version of the rhs, once $V_{\Sigma_g^+}$, $V_{\Sigma_u^-}$, and V_{Π_u} are known. In the following sections, we are going to derive short and long distance constraints on these potentials using weak coupling pNRQCD [6,12] and the QCD effective string theory [13,14] respectively.

1. Short distance constraints

At short distances, the time evolution of a $Q\bar{Q}$ pair is described by the weak coupling regime of pNRQCD [6,12], the Lagrangian of which has been displayed in (15) at next-to-leading order in the multipole expansion. The operators $\hat{O}(\mathbf{r},\mathbf{R},t)$ and $\hat{O}_B^i(\mathbf{r},\mathbf{R},t)$ match onto the singlet field $S(\mathbf{r},\mathbf{R},t)$ and the operator $\mathrm{tr}(O(\mathbf{r},\mathbf{R},t)B^i(\mathbf{R},t))$ respectively. The leading spin-dependent term in the pNRQCD Lagrangian reads [25]

$$\begin{aligned}\mathcal{L}'_{\mathrm{pNRQCD}} &= \frac{gc_F}{2m_Q}\mathrm{Tr}(\mathrm{O}^\dagger(\mathbf{r},\mathbf{R},t)\mathbf{B}(\mathbf{R},t)\{\boldsymbol{\sigma},\mathrm{S}(\mathbf{r},\mathbf{R},t)\})\\ &\quad+\mathrm{H.c.}.\end{aligned} \quad (30)$$

We use tr for the trace over color indices and Tr for the trace over both color and spin indices. Notice that the term above

shows an $\mathbf{r}$-independent interaction between the singlet field and the operator $\mathrm{tr}(OB^i)$, which implies that

$$V_S^\Sigma(r) = V_S^\Pi(r) = \pm\frac{c_F\lambda^2}{m_Q}, \tag{31}$$

where $\lambda \sim \Lambda_{\rm QCD}$ is a constant, and we have put the sign explicitly.

2. Long distance constraints

At long distances, the energy spectrum of a static $Q\bar{Q}$ pair is well described by the QCD effective string theory (EST) [13,14]. The mapping between operator insertions in the temporal Wilson lines of the Wilson loop and the corresponding operators in the EST was established in Ref. [26], following earlier work [27]. For the relevant operators to us, it reads

$$\begin{aligned}
B^l(t,\mathbf{r}/2) &\to \Lambda'\epsilon^{lm}\partial_t\partial_z\xi^m(t,r/2)\\
B^l(t,-\mathbf{r}/2) &\to \Lambda'\epsilon^{lm}\partial_t\partial_z\xi^m(t,-r/2)\\
B^3(t,\mathbf{r}/2) &\to \Lambda'''\epsilon^{lm}\partial_t\partial_z\xi^l(t,r/2)\partial_z\xi^m(t,r/2)\\
B^3(t,-\mathbf{r}/2) &\to \Lambda'''\epsilon^{lm}\partial_t\partial_z\xi^l(t,-r/2)\partial_z\xi^m(t,-r/2),
\end{aligned} \tag{32}$$

where $l,m=1,2$. Here, we also need to map the states created by operator insertions in spacial Wilson lines to the corresponding states in EST. In order to do so, it is convenient to take the $\mathbf{r}$ along the z axis and write the EST Lagrangian in terms of the complex field $\varphi(z,t) = (\xi^1(z,t) + i\xi^2(z,t))/\sqrt{2}$. This field has nice transformation properties under $D_{\infty h}$, the relevant space group,

$$\begin{aligned}
R_z(\theta)&:\ \varphi(z,t) \to e^{i\theta}\varphi(z,t)\\
P&:\ \varphi(z,t) \to -\varphi(-z,t)\\
R_{xz}&:\ \varphi(z,t) \to \varphi^*(z,t),
\end{aligned} \tag{33}$$

where $R_z(\theta), P$, and R_{xz} stand for a rotation of angle θ around the z axis, a parity transformation, and a reflection through the xz plain respectively. The Lagrangian density at leading order reads

$$\mathcal{L}_{\rm EST} = \kappa\partial_\mu\varphi\partial^\mu\varphi^*, \tag{34}$$

where κ is the string tension and $\varphi(z,t)$ fulfills Dirichlet boundary conditions, $\varphi(r/2,t) = \varphi(-r/2,t) = 0$. $\varphi(z,t)$ can written in terms of creation and annihilation operators:

$$\begin{aligned}
\varphi(z,t) &= \sum_{n=1}^{\infty}\frac{1}{2E_n}(e^{-iE_nt}\varphi_n(z)a_n + e^{iE_nt}\varphi_n^*(z)b_n^\dagger)\\
\varphi_n(z) &= \frac{1}{\sqrt{2r}}(e^{iE_nz} + (-1)^{n+1}e^{-iE_nz})\\
[a_n,a_m^\dagger] &= [b_n,b_m^\dagger] = \frac{2E_n}{\kappa}\delta_{nm}, \qquad E_n = \frac{\pi n}{r}.
\end{aligned} \tag{35}$$

The remaining commutators vanish. $a_n^\dagger$ ($b_n^\dagger$) on the vacuum creates a state of energy E_n, angular momentum 1 (-1) and parity $(-1)^n$. The reflection with respect to the xz plain interchanges $a_n \leftrightarrow b_n$. If we define

$$\begin{aligned}
\hat{O}_B^\dagger(\mathbf{r},\mathbf{0},t) &= \hat{O}_B^{\dagger 1}(\mathbf{r},\mathbf{0},t) + i\hat{O}_B^{\dagger 2}(\mathbf{r},\mathbf{0},t)\\
\hat{O}_B^{\dagger *}(\mathbf{r},\mathbf{0},t) &= \hat{O}_B^{\dagger 1}(\mathbf{r},\mathbf{0},t) - i\hat{O}_B^{\dagger 2}(\mathbf{r},\mathbf{0},t),
\end{aligned} \tag{36}$$

then the following identifications fulfill the $D_{\infty h}$ symmetry requirements,

$$\begin{aligned}
&\hat{O}^\dagger(\mathbf{r},\mathbf{0},-T/2)|0\rangle \to |0\rangle\\
&\hat{O}_B^{\dagger 3}(\mathbf{r},\mathbf{0},-T/2)|0\rangle \to \frac{\kappa}{2\sqrt{2E_1E_2}}(a_1^\dagger b_2^\dagger - b_1^\dagger a_2^\dagger)|0\rangle\\
&\hat{O}_B^\dagger(\mathbf{r},\mathbf{0},-T/2)|0\rangle \to \sqrt{\frac{\kappa}{2E_1}}b_1^\dagger|0\rangle\\
&\hat{O}_B^{\dagger *}(\mathbf{r},\mathbf{0},-T/2)|0\rangle \to -\sqrt{\frac{\kappa}{2E_1}}a_1^\dagger|0\rangle.
\end{aligned} \tag{37}$$

Let us perform analogous definitions for the chromomagnetic fields,

$$\begin{aligned}
B(t,\mathbf{r}) &= B^1(t,\mathbf{r}) + iB^2(t,\mathbf{r})\\
B^*(t,\mathbf{r}) &= B^1(t,\mathbf{r}) - iB^2(t,\mathbf{r}).
\end{aligned} \tag{38}$$

The mapping (32) then reads

$$\begin{aligned}
B(t,\pm\mathbf{r}/2) &\to -i\sqrt{2}\Lambda'\partial_t\partial_z\varphi(\pm r/2,t)\\
B^*(t,\pm\mathbf{r}/2) &\to i\sqrt{2}\Lambda'\partial_t\partial_z\varphi^*(\pm r/2,t)\\
B^3(t,\pm\mathbf{r}/2) &\to i\Lambda'''\partial_t\partial_z\varphi(\pm r/2,t)\partial_z\varphi^*(\pm r/2,t) + \text{H.c.}.
\end{aligned} \tag{39}$$

Upon substituting the above expressions and (37) in (28), we obtain

$$V_S^\Sigma(r) = -\frac{\pi^2 g\Lambda''' c_F}{m_Q\kappa r^3}, \qquad V_S^\Pi(r) = \frac{\pi^{3/2} g\Lambda' c_F}{2m_Q\sqrt{\kappa}r^2}. \tag{40}$$

The parameters $g\Lambda' \sim \Lambda_{\rm QCD}$ and $g\Lambda''' \sim \Lambda_{\rm QCD}$ also appear in the spin-orbit and tensor potentials of a heavy quarkonium [26,28], which have been calculated on the lattice [24,29]. We obtain from fits to the data of Ref. [30]

$$g\Lambda' \sim -59\ \text{MeV}, \qquad g\Lambda''' \sim \pm 230\ \text{MeV}. \tag{41}$$

Details on the fits are given in Appendix B[2]

3. Modeling the mixing potential

For the actual mixing potentials, we use a simple interpolation between (31) and (40) that allows for a sign

[2]Due to an error in the identification, the value of $g\Lambda'$ displayed in Ref. [11] as Λ' is twice the actual value. This change does not affect the statements made in that paper.

flip between the short and long distance expressions without introducing any further scale, namely,

$$V_S^{\Pi}[\pm-](r) = \frac{\lambda^2}{m_Q}\left(\frac{\pm 1-(\frac{r}{r_\Pi})^2}{1+(\frac{r}{r_\Pi})^4}\right) \tag{42}$$

$$V_S^{\Sigma}[\pm\pm](r) = \frac{\lambda^2}{m_Q}\left(\frac{\pm 1\pm(\frac{r}{r_\Sigma})^2}{1+(\frac{r}{r_\Sigma})^5}\right), \tag{43}$$

where $r_\Pi = (\frac{|g\Lambda'|\pi^{\frac{3}{2}}}{2\lambda^2\kappa^{\frac{1}{2}}})^{\frac{1}{2}}$ and $r_\Sigma = (\frac{|g\Lambda'''|\pi^2}{\lambda^2\kappa})^{\frac{1}{3}}$. Note that the $\pm$ in V_S^Π and the first $\pm$ in V_S^Σ are correlated because both potentials have the same short distance behavior. We will explore the following values for the only unknown parameter λ, $\lambda = 100$, 300, 600 MeV, and all possible sign combinations for the 1^{--} charmonium states below and choose the one that suits the phenomenology best.

B. Mixing equations

Now, we need to include the quark spin degree of freedom in the equations displayed in Sec. II. Let us write

$$S = \frac{1}{\sqrt{2}}(S_0 + \sigma^k S_1^k)$$
$$H^j = \frac{1}{\sqrt{2}}(H_0^j + \sigma^i H_1^{ji}), \tag{44}$$

where we have omitted the arguments in $S = S(\mathbf{R},\mathbf{r},t)$ and $H^j = H^j(\mathbf{R},\mathbf{r},t)$, the subscripts 0 and 1 stand for the total spin of the quark-antiquark pair, and the superscripts k and i label the three states in the spin 1 case. Recall that the superscript j labels the three states of the total angular momentum 1 of the gluonic degrees of freedom. Then, the last term in (18) reads

$$\mathrm{tr}(S^\dagger V_S^{ij}\{\sigma^i, H^j\}) = 2V_S^{ij}(S_1^{i\,\dagger}H_0^j + S_0{}^\dagger H_1^{ji}). \tag{45}$$

Note that this term mixes spin 0 (1) hybrids with a spin 1 (0) quarkonium. In view of the decomposition of V_S^{ij} in (19), we only need to analyze $S_1^{j\,\dagger}H_0^j$, $S_1^{i\,\dagger}H_0^j\hat{r}^i\hat{r}^j$, $S_0{}^\dagger H_1^{ji}$, and $S_0{}^\dagger H_1^{ji}\hat{r}^i\hat{r}^j$. Consider the first expression,

$$\int d\Omega S_1^{j\,\dagger}H_0^j = \sum_{JML}\frac{S_{1JM}^{L\dagger}P_{0JM}^L}{r^2} = \sum_{\mathcal{J}\mathcal{M}L}\frac{S_{1\mathcal{J}\mathcal{M}}^{L\dagger}P_{0\mathcal{J}\mathcal{M}}^L}{r^2}, \tag{46}$$

where J is the orbital angular momentum, plus the quark spin for S_1 and plus the gluonic total angular momentum for H_0, and M is its third component. $J = \mathcal{J}$ and $M = \mathcal{M}$ are the total angular momentum and its third component respectively. $L = J$, $J \pm 1$ are simply denoted by $0, \pm$. We have used above the same decomposition for S_1^j as the one used for H^j in (4). For the second expression, we have

$$\int d\Omega S_1^{i\,\dagger}H_0^j\hat{r}^i\hat{r}^j = \frac{1}{r^2}S_{1\mathcal{J}\mathcal{M}}^{-\dagger}\left(\frac{\mathcal{J}}{2\mathcal{J}+1}P_{0\mathcal{J}\mathcal{M}}^- - \frac{\sqrt{\mathcal{J}(\mathcal{J}+1)}}{2\mathcal{J}+1}P_{0\mathcal{J}\mathcal{M}}^+\right)$$
$$+\frac{1}{r^2}S_{1\mathcal{J}\mathcal{M}}^{+\dagger}\left(\frac{\mathcal{J}+1}{2\mathcal{J}+1}P_{0\mathcal{J}\mathcal{M}}^+ - \frac{\sqrt{\mathcal{J}(\mathcal{J}+1)}}{2\mathcal{J}+1}P_{0\mathcal{J}\mathcal{M}}^-\right). \tag{47}$$

For the third and fourth expressions, we need to introduce tensor spherical harmonics $Y_{\mathcal{J}\mathcal{M}}^{jiLJ}(\hat{\mathbf{r}})$ (see Appendix C), which are eigenfunctions of $\mathbf{S}^2$, $\mathbf{L}_g^2$, $\mathbf{L}^2$, $\mathbf{J}^2$, $\boldsymbol{\mathcal{J}}^2$, and $\mathcal{J}_3$ with eigenvalues 2, 2, $L(L+1)$, $J(J+1)$, $\mathcal{J}(\mathcal{J}+1)$, and $\mathcal{M}$ respectively, with $L = J$, $J \pm 1$, $J = \mathcal{J}$, $\mathcal{J} \pm 1$. We then have

$$H_1^{ji}(\mathbf{r},t) = \frac{1}{r}\sum_{LJ\mathcal{J}\mathcal{M}}Y_{\mathcal{J}\mathcal{M}}^{jiLJ}(\hat{\mathbf{r}})P_{1\mathcal{J}\mathcal{M}}^{LJ}(r). \tag{48}$$

We will use $0, \pm$ both for $L = J$, $J \pm 1$ and $J = \mathcal{J}$, $\mathcal{J} \pm 1$. Hence,

$$\int d\Omega S_0{}^\dagger H_1^{jj} = \frac{1}{r^2}\sum_{\mathcal{J}\mathcal{M}}S_{0\mathcal{J}\mathcal{M}}^\dagger\left(-\sqrt{\frac{2\mathcal{J}-1}{2\mathcal{J}+1}}P_{1\mathcal{J}\mathcal{M}}^{+-} + P_{1\mathcal{J}\mathcal{M}}^{00} - \sqrt{\frac{2\mathcal{J}+3}{2\mathcal{J}+1}}P_{1\mathcal{J}\mathcal{M}}^{-+}\right) \tag{49}$$

$$\int d\Omega S_0{}^\dagger H_1^{ji}\hat{r}^i\hat{r}^j = \frac{1}{r^2}\sum_{\mathcal{J}\mathcal{M}}S_{0\mathcal{J}\mathcal{M}}^\dagger \times \left(\sqrt{\frac{\mathcal{J}(\mathcal{J}-1)}{(2\mathcal{J}+1)(2\mathcal{J}-1)}}P_{1\mathcal{J}\mathcal{M}}^{--} - \frac{\mathcal{J}}{\sqrt{(2\mathcal{J}+3)(2\mathcal{J}+1)}}P_{1\mathcal{J}\mathcal{M}}^{+-}\right.$$
$$\left.+\sqrt{\frac{(\mathcal{J}+1)(\mathcal{J}+2)}{(2\mathcal{J}+1)(2\mathcal{J}+3)}}P_{1\mathcal{J}\mathcal{M}}^{++} - \frac{\mathcal{J}+1}{\sqrt{(2\mathcal{J}+3)(2\mathcal{J}+1)}}P_{1\mathcal{J}\mathcal{M}}^{-+}\right). \tag{50}$$

Putting all together, we get the following sets of coupled equations. For $S=0$ hybrids, we have for $\mathcal{J}\neq 0$

$$\left[-\frac{1}{m_Q}\frac{\partial^2}{\partial r^2}+\frac{\mathcal{J}(\mathcal{J}+1)}{m_Q r^2}+\begin{pmatrix} V_{\Sigma_g^+} & 2V_S^\Pi \\ 2V_S^\Pi & V_{\Pi_u}\end{pmatrix}\right]\begin{pmatrix} S^0_{1\mathcal{J}\mathcal{M}}(r) \\ P^0_{0\mathcal{J}\mathcal{M}}(r)\end{pmatrix}=E\begin{pmatrix} S^0_{1\mathcal{J}\mathcal{M}}(r) \\ P^0_{0\mathcal{J}\mathcal{M}}(r)\end{pmatrix}, \tag{51}$$

$$\left[-\frac{1}{m_Q}\frac{\partial^2}{\partial r^2}+\begin{pmatrix} \frac{(\mathcal{J}+1)(\mathcal{J}+2)}{m_Q r^2}+V_{\Sigma_g^+} & 0 & 2\left(V_S^\Pi+\frac{\mathcal{J}+1}{2\mathcal{J}+1}V_S^q\right) & -2V_S^q\frac{\sqrt{\mathcal{J}(\mathcal{J}+1)}}{2\mathcal{J}+1} \\ 0 & \frac{(\mathcal{J}-1)\mathcal{J}}{m_Q r^2}+V_{\Sigma_g^+} & -2V_S^q\frac{\sqrt{\mathcal{J}(\mathcal{J}+1)}}{2\mathcal{J}+1} & 2\left(V_S^\Pi+\frac{\mathcal{J}}{2\mathcal{J}+1}V_S^q\right) \\ 2\left(V_S^\Pi+\frac{\mathcal{J}+1}{2\mathcal{J}+1}V_S^q\right) & -2\frac{\sqrt{\mathcal{J}(\mathcal{J}+1)}}{2\mathcal{J}+1} & \frac{(\mathcal{J}+1)(\mathcal{J}+2)}{m_Q r^2}+V_{\Sigma_u^-}+\frac{\mathcal{J}}{2\mathcal{J}+1}V_q & \frac{\sqrt{\mathcal{J}(\mathcal{J}+1)}}{2\mathcal{J}+1}V_q \\ -2V_S^q\frac{\sqrt{\mathcal{J}(\mathcal{J}+1)}}{2\mathcal{J}+1} & 2\left(V_S^\Pi+\frac{\mathcal{J}}{2\mathcal{J}+1}V_S^q\right) & \frac{\sqrt{\mathcal{J}(\mathcal{J}+1)}}{2\mathcal{J}+1}V_q & \frac{(\mathcal{J}-1)\mathcal{J}}{m_Q r^2}+V_{\Sigma_u^-}+\frac{\mathcal{J}+1}{2\mathcal{J}+1}V_q\end{pmatrix}-E\right] \times\begin{pmatrix} S^+_{1\mathcal{J}\mathcal{M}}(r) \\ S^-_{1\mathcal{J}\mathcal{M}}(r) \\ P^+_{0\mathcal{J}\mathcal{M}}(r) \\ P^-_{0\mathcal{J}\mathcal{M}}(r)\end{pmatrix}=0, \tag{52}$$

where $V_S^q=V_S^\Sigma-V_S^\Pi$. For $\mathcal{J}=0$, Eqs. (51) do not exist, and Eqs. (52) reduce to two coupled equations for $S^+_{100}(r)$ and $P^+_{000}(r)$. For $S=1$ hybrids, $P^{+0}_{1\mathcal{J}\mathcal{M}}(r)$ and $P^{-0}_{1\mathcal{J}\mathcal{M}}(r)$ do not couple to heavy quarkonium. The remaining do it according to the following equations for $\mathcal{J}>1$,

$$\left[\frac{1}{m_Q}\frac{\partial^2}{\partial r^2}-\begin{pmatrix} \frac{\mathcal{J}(\mathcal{J}+1)}{m_Q r^2}+V_{\Sigma_g^+} & V_S^{++} & V_S^{-+} & V_S^{+-} & V_S^{--} & V_S^\Pi \\ V_S^{++} & \frac{(\mathcal{J}+2)(\mathcal{J}+3)}{m_Q r^2}+V^{++} & -2V_q\frac{\sqrt{(\mathcal{J}+1)(\mathcal{J}+2)}}{2\mathcal{J}+3} & 0 & 0 & 0 \\ V_S^{-+} & -2V_q\frac{\sqrt{(\mathcal{J}+1)(\mathcal{J}+2)}}{2\mathcal{J}+3} & \frac{\mathcal{J}(\mathcal{J}+1)}{m_Q r^2}+V^{-+} & 0 & 0 & 0 \\ V_S^{+-} & 0 & 0 & \frac{\mathcal{J}(\mathcal{J}+1)}{m_Q r^2}+V^{+-} & V_q\frac{\sqrt{(\mathcal{J}-1)\mathcal{J}}}{2\mathcal{J}-1} & 0 \\ V_S^{--} & 0 & 0 & V_q\frac{\sqrt{(\mathcal{J}-1)\mathcal{J}}}{2\mathcal{J}-1} & \frac{(\mathcal{J}-1)\mathcal{J}}{m_Q r^2}+V^{--} & 0 \\ V_S^\Pi & 0 & 0 & 0 & 0 & \frac{\mathcal{J}(\mathcal{J}+1)}{m_Q r^2}+V_{\Pi_u}\end{pmatrix}+E\right] \times\begin{pmatrix} S_{0\mathcal{J}\mathcal{M}}(r) \\ P^{++}_{1\mathcal{J}\mathcal{M}}(r) \\ P^{-+}_{1\mathcal{J}\mathcal{M}}(r) \\ P^{+-}_{1\mathcal{J}\mathcal{M}}(r) \\ P^{--}_{1\mathcal{J}\mathcal{M}}(r) \\ P^{00}_{1\mathcal{J}\mathcal{M}}(r)\end{pmatrix}=0, \tag{53}$$

where

TABLE IV. Spectrum of charmonium ($S=1$) and charmonium hybrids ($S=0$): 1^{--} states. Masses are in GeV. The % columns show the fraction of the hybrid components for the mass states in the previous column. $m_c = 1.47$ GeV.

			$V_S^\Pi[+-]$, $V_S^\Sigma[++]$				$V_S^\Pi[+-]$, $V_S^\Sigma[+-]$				$V_S^\Pi[--]$, $V_S^\Sigma[-+]$				$V_S^\Pi[--]$, $V_S^\Sigma[--]$			
NL_J	$\lambda=0$	%	$\lambda=0.3$	%	$\lambda=0.6$	%	$\lambda=0.3$	%	$\lambda=0.6$	%	$\lambda=0.3$	%	$\lambda=0.6$	%	$\lambda=0.3$	%	$\lambda=0.6$	%
$1s$	3.068	0	3.064	0	3.001	4	3.066	0	3.053	0	3.063	0	3.036	2	3.061	1	2.989	6
$2s$	3.678	0	3.672	1	3.628	14	3.677	1	3.670	4	3.677	0	3.661	4	3.672	1	3.630	7
$1d$	3.793	0	3.773	4	3.687	12	3.790	1	3.785	2	3.792	0	3.789	0	3.782	1	3.712	7
$1(s/d)_1$	4.011	100	4.016	96	4.014	71	4.012	99	4.004	96	4.014	99	4.025	99	4.016	98	4.040	85
$3s$	4.131	0	4.127	0	4.107	10	4.128	1	4.130	7	4.130	0	4.125	10	4.128	2	4.103	12
$2d$	4.210	0	4.203	20	4.180	79	4.209	10	4.207	39	4.209	2	4.205	5	4.204	1	4.172	52
$2(s/d)_1$	4.355	100	4.358	97	4.366	65	4.356	98	4.355	89	4.357	100	4.368	94	4.357	100	4.383	86
$4s$	4.512	0	4.515	0	4.497	0	4.517	1	4.513	7	4.517	0	4.508	8	4.515	1	4.495	0
$3d$	4.579	0	4.573	2	4.559	8	4.578	0	4.574	5	4.578	1	4.568	7	4.574	0	4.550	3
$3(s/d)_1$	4.692	100	4.699	98	4.711	83	4.694	99	4.699	93	4.693	100	4.699	97	4.698	99	4.724	90
$4(s/d)_1$	4.718	100	4.730	100	4.785	96	4.719	100	4.718	98	4.720	100	4.728	98	4.728	100	4.779	97
$5s$	4.865	0	4.864	0	4.848	3	4.865	0	4.865	7	4.865	0	4.867	7	4.864	1	4.846	2
$4d$	4.916	0	4.913	7	4.903	35	4.915	2	4.915	19	4.915	0	4.912	12	4.913	3	4.894	21
$5(s/d)_1$	5.043	100	5.044	99	5.046	84	5.043	99	5.043	94	5.044	100	5.050	97	5.044	100	5.067	93

$$V_S^{++} = \sqrt{\frac{(\mathcal{J}+1)(\mathcal{J}+2)}{(2\mathcal{J}+1)(2\mathcal{J}+3)}} V_S^q$$

$$V_S^{-+} = -\frac{\mathcal{J}+1}{\sqrt{(2\mathcal{J}+3)(2\mathcal{J}+1)}} V_S^q - \sqrt{\frac{2\mathcal{J}+3}{2\mathcal{J}+1}} V_S^\Pi$$

$$V_S^{+-} = -\frac{\mathcal{J}}{\sqrt{(2\mathcal{J}+3)(2\mathcal{J}-1)}} V_S^q - V_S^\Pi \frac{\sqrt{(2\mathcal{J}-1)(2\mathcal{J}+1)}}{2\mathcal{J}+1}$$

$$V_S^{--} = \sqrt{\frac{\mathcal{J}(\mathcal{J}-1)}{(2\mathcal{J}+1)(2\mathcal{J}-1)}} V_S^q$$

$$V^{++} = V_{\Sigma_u^-} + \frac{\mathcal{J}+1}{2\mathcal{J}+3} V_q$$

$$V^{-+} = V_{\Sigma_u^-} + \frac{\mathcal{J}+2}{2\mathcal{J}+3} V_q$$

$$V^{+-} = V_{\Sigma_u^-} + \frac{\mathcal{J}-1}{2\mathcal{J}-1} V_q$$

$$V^{--} = V_{\Sigma_u^-} + \frac{\mathcal{J}}{2\mathcal{J}-1} V_q. \tag{54}$$

For $\mathcal{J}=0$, $P_{100}^{00}(r)$, $P_{100}^{--}(r)$, and $P_{100}^{+-}(r)$ do not exist, and the system reduces to the three upper equations. $P_{100}^{0-}(r)$, which does not couple to a heavy quarkonium, does not exist, either. For $\mathcal{J}=1$, $P_{11\mathcal{M}}^{--}(r)$ does not exist, and the system above reduces to five coupled equations.

C. Spectrum

In order to fix the signs and the parameter λ of the mixing potentials, we focus on the spin zero $n(s/d)_1$ ($n=1,2,3$) states in Table I, which can be identified with $Y(4008)$, $Y(4360)$, and $Y(4660)$. The main problem with this identification is that all three states have been observed to decay to spin 1 quarkonium states, which violates spin symmetry. However, according to Eq. (52), the spin zero hybrids mix with spin 1 quarkonium, and hence, if this mixing is large, we may find a natural explanation to these decays. We present our results in Table IV (the case $\lambda=100$ MeV is not displayed; it produces a tiny mixing in all cases). We observed that the case that provides the largest amount of mixing is the combination $V_S^\Pi[+-]$ with $V_S^\Sigma[++]$ and $\lambda=600$ MeV. This is the sign combination and the value of λ that we will take for the rest of the paper. The spectrum of charmonium and charmonium hybrids is given in Tables IV–XII, and the one of bottomonium and bottomonium hybrids is given in Tables XIII–XX. The general trend (with a few exceptions) is that hybrid states get heavier whereas quarkonium states get lighter due the mixing.

Since we have used the leading order potential for both quarkonium and hybrids, the potentials we missed start at order $1/m_Q$. Hence, the error to assign to this calculation for the hybrids is $\Lambda_{\rm QCD}^2/m_Q$, since $\Lambda_{\rm QCD}$ is the next relevant scale. For a quarkonium, this is not always the case, since the typical momenta can be larger than $\Lambda_{\rm QCD}$. A detailed error analysis is carried out in the Appendix A. For simplicity, we will stick to the $\Lambda_{\rm QCD}^2/m_Q$ estimate for quarkonium as well. Taking $\Lambda_{\rm QCD}\sim 400$ MeV, we obtain a precision of about 110 MeV for charmonium and 33 MeV for bottomonium. These are the numbers we will have in mind when comparing to experiment and to other approaches.

V. COMPARISON WITH OTHER APPROACHES

In this section, we compare our results with other QCD-based approaches. For convenience, we will compare our

results for the spectrum in the case $\lambda = 0$ (no mixing). The shifts in the spectrum due to mixing are within our estimated errors.

A. Born-Oppenheimer approximation

In Ref. [4], the lower lying bottomonium hybrid spectrum was calculated from the static potentials Π_u and Σ_u^- and normalized to the bottomonium spectrum. The mixing between hybrid states built out of these potentials that appears at leading order due to the kinetic term of the heavy quarks was ignored. The masses obtained for H_1 $(1(s/d)_1)$, H_2 $(1p_1)$, H_3 $(1p_0)$, and H_1' $(2(s/d)_1)$ are between 150 and 300 MeV heavier than ours. This is probably due to the different choice of the bottom quark mass.

In Ref. [9], the lower lying hybrid spectrum was calculated as above. However, for charmonium, the ground state for each potential was fixed to the lattice data of Ref. [31]. The mixing between hybrid states was also ignored. If we compare the splittings obtained from Table X of Ref. [9] with those obtained from our Tables I and II, we find agreement within 20 MeV, except for the H_4-H_1 case for which we obtain a lower value by about 40 MeV and the $H_3' - H_3$ case for which we obtain a higher value of about 70 MeV. We have identified the states H_1, H_1', H_2, H_2', H_2'', $H_3(1P)$, and H_4 with $1(s/d)_1$, $2(s/d)_1$, $1p_1$, $1d_2$, $2p_1$, $3(s/d)_1$, and $1(p/f)_2$ respectively.

Our hybrid spectrum is compatible within errors with that of Ref. [10] both for charmonium and bottomonium, except for the bottomonium $1(s/d)_1$ and $2p_0$ states, for which we have slightly lower masses. Our central values tend to be at the lower end of their error bars. Although the construction of the effective theory for hybrids is somewhat different and the parametrization of the potentials is as well, the most relevant difference is probably the normalization of the spectrum. Indeed, in Ref. [10], the hybrid spectrum is normalized using the charm and bottom masses in the renormalon subtraction (RS) scheme [32], whereas here we normalize it to the corresponding quarkonium spectrum, which is not calculated in that reference. We have checked that we reproduce the results of Ref. [10] with our code if we input their potentials.[3]

B. Lattice QCD

In Ref. [33], the spectrum of the lightest exotic charmonium hybrids is calculated in the quenched approximation for a relativistic charm action in an anisotropic lattice ($a_s = 0.197 - 0.09$ fm, $a_s/a_t = 2$). Their results for the 1^{-+}, 0^{+-}, and 2^{+-} states are between 400 and 700 MeV higher than ours.

[3]We have also checked that our results are reproduced by the code of Ref. [10] if our potentials are input. We thank the authors of that reference for providing their code for the test.

There has been a recent update [34] of earlier results [31] by the Hadronic Spectrum Collaboration for the charmonium spectrum including hybrid states. They use relativistic charm and dynamical light quarks in an anisotropic lattice with temporal spacing $a_t \sim 0.034$ fm and spatial spacing $a_s \sim 0.12$ fm. The update basically consists of taking up and down quark masses smaller than in the previous calculation ($m_\pi \sim 240$ MeV and $m_\pi \sim 400$ MeV respectively). The hierarchy of the lowest lying hybrid multiplets agrees with ours, from lighter to heavier: $1(s/d)_1$, $1p_1$, $1(p/f)_2$, and $1p_0$. However, their numbers are considerably larger than ours: 381, 326, 392, and 151 MeV higher for the spin average of the $1(s/d)_1$, $1p_1$, $1(p/f)_2$, and $1p_0$ multiplets respectively. The hierarchy in which quarkonium and hybrid states arise agrees for the 1^{++} (four states) and 1^{+-} (six states) quantum numbers but disagrees for the remaining nonexotic ones.

In Ref. [35], the lower lying charmonium spectrum is also calculated with four dynamical quarks in a Wilson twisted mass action. Lattice spacings ranging from 0.0619 fm to 0.0885 fm and pion masses ranging from 225 to 470 MeV are used, and both the continuum and the chiral extrapolations are carried out. They find a 1^{--} state at 3951 MeV that is compatible with our $1(s/d)_1$ spin zero hybrid state (4011 MeV). With less significance, they also find two 2^{++} states at about 4460 and 4530 MeV which are compatible with our $2f$ quarkonium (4428 MeV) and $2(p/f)_2$ spin zero hybrid (4563 MeV) respectively.

In Ref. [4], the bottomonium hybrid spectrum is calculated in quenched lattice NRQCD using an anisotropic lattice ($a_s \sim 0.11$ fm, $a_s/a_t = 3$). They find the lightest hybrid H_1 $(1(s/d)_1)$ 1.49(2)(5) GeV above the $1S$ quarkonium; this is about 250 MeV heavier than ours. About the same difference is also found for H_2 $(1p_1)$ and H_3 $(1p_0)$, whereas for H_1' $(2(s/d)_1)$, the difference rises to 470 MeV.

For the bottomonium, there is also a quenched lattice calculation with relativistic bottom quarks in an anisotropic lattice ($a_s \sim 0.04$–0.17 fm, $a_s/a_t = 4, 5$) [36]. The masses for the lightest 2^{--}, 1^{-+}, and 2^{+-} hybrids are displayed, which turn out to be either lighter (2^{--}) or heavier (1^{-+} and 2^{+-}) than our results, in spite of the large errors (200–600 MeV).

C. QCD sum rules

In Ref. [37], the hybrid spectrum for charmonium and bottomonium is calculated.

For charmonium, the quantum numbers of their lightest hybrid multiplet coincide with ours $(1(s/d)_1)$, and the masses are compatible with ours for the 1^{-+} and 2^{-+} states within errors (between 150 and 230 MeV), but below for the 0^{-+} and 1^{--} states. For spin zero hybrids, they obtain a 2^{++} state $(1(p/f)_2)$ as the second lighter state, whereas we

have a 1^{++} state ($1p_1$). The mass of the 2^{++} state is, nevertheless, compatible with ours within the large errors, but the masses of the 1^{++} and 0^{++} states are higher. The masses of the spin 1 hybrids 0^{+-} and 1^{+-} are compatible, again within large errors.

For the bottomonium, they obtain the same hierarchy of multiplets as in the charmonium. However, the larger errors make it now compatible with ours, even though the central values are not. The masses of the lightest multiplet are considerably lower than ours, but the ones of the remaining multiplets (1^{++}, 0^{+-}, 1^{+-}; 2^{++}; 0^{++}) are compatible within large errors.

VI. COMPARISON WITH EXPERIMENT

In this section, we compare experimental results with ours in the case of maximum mixing, that is, with the results displayed on the sixth column of Table IV and on the fourth column of Tables VI–XX. As mentioned before, the shifts in the spectrum due to mixing are not very important. However, the violations of heavy quark spin symmetry induced by the mixing are crucial to map our results to the XYZ states. We omit in the analysis the neutral states that have been identified as isospin partners of charged states.

A. Charm

(i) $X(3823)$ [18] is compatible with our 2^{--} charmonium $1d$ state (3792 MeV).

(ii) $X(3872)$ [18] is compatible with our 1^{++} charmonium $2p$ states (3967 MeV). Since it sits at the $D^0\bar{D}^{0*}$ threshold, it is expected to have a large mixing with those states that we have not taken into account.

(iii) $X(3915)$ and $X(3940)$ [18] are also compatible with our charmonium $2p$ states (3968 MeV). Since they are close to the $D_s\bar{D}_s$ threshold (3936 MeV), the 0^+ states may have a large mixing with those states.

(iv) $Y(4008)$ [38] is compatible with our 1^{--} hybrid $1(s/d)_1$ (H_1) state (4004 MeV). It mixes with a spin 1 charmonium (see column 7 in Table IV and Fig. 6), which may explain the observed spin symmetry violating decays.

(v) $X(4140)$ [39] and $X(4160)$ [18] are compatible with our 1^{++} hybrid $1p_1$ (H_2) state (4146 MeV). Since the quantum numbers of $X(4160)$ have not been established, it may also correspond to the $1(p/f)_2$ hybrid or to the scalar $3s$ or $2d$ states. The fact that no decays to charmonium of the $1p_1$ state are allowed at leading order is consistent with the fact that no such decays have been observed so far for $X(4160)$, which selects it as our favorite hybrid candidate for that state. If so, there is no room for the $X(4140)$ (1^{++}) in our spectrum. These states may be affected by the $D_s^*\bar{D}_s$ threshold (4080 MeV).

(vi) $X(4230)$ and $Y(4260)$ [18] are compatible with our 1^{--} charmonium $2d$ state (4180 MeV). It may have a dominant spin zero hybrid component (see Table IV), which may help us to understand the recent results by the BESSIII Collaboration [40]. Indeed, in Ref. [41], it is claimed that the former $Y(4260)$ peak observed in $\pi^+\pi^- J/\psi$ invariant mass actually consists of two resonances $Y(4220)$ and $Y(4390)$. The parameters of the first resonance are compatible with the ones of $X(4230)$. They are also compatible with the ones of one of the structures observed in $\pi^+\pi^- h_c$ [42]. The large hybrid component (see Fig. 7) may explain why it is also observed in this second channel, which would be suppressed by spin symmetry otherwise. It may also be affected by the $D_1\bar{D}$ threshold (4290 MeV).

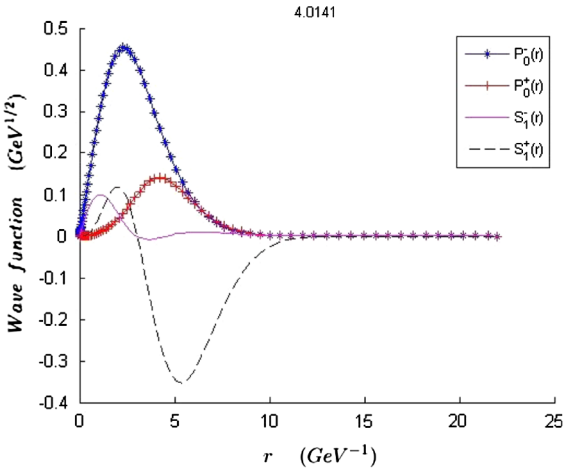

FIG. 6. The wave function of the charmonium 1^{--} $1(s/d)_1$ state.

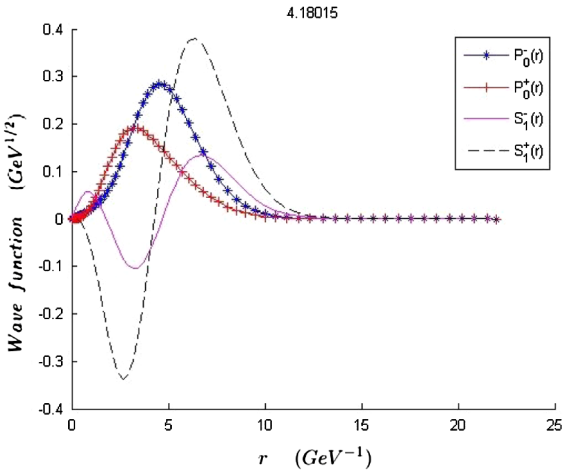

FIG. 7. The wave function of the charmonium 1^{--} $2d$ state.

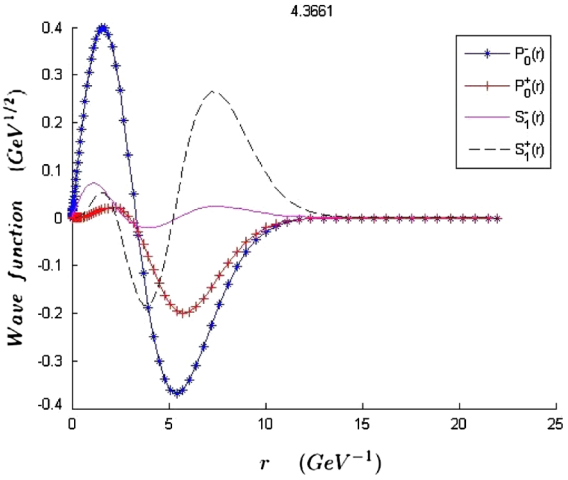

FIG. 8. The wave function of the charmonium 1^{--} $2(s/d)_1$ state.

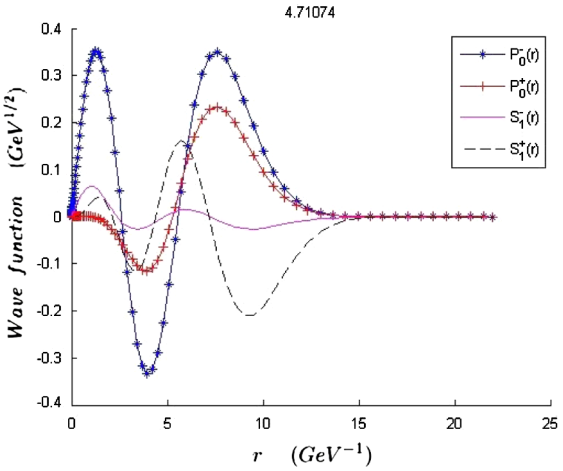

FIG. 10. The wave function of the charmonium 1^{--} $3(s/d)_1$ state.

(vii) $Y(4274)$ [39] is compatible with our 1^{++} charmonium $3p$ state (4368 MeV). It may be affected by the $D_s^*\bar{D}_s^*$ threshold (4224 MeV).

(viii) $X(4350)$ [18] is compatible with our spin 1 $2(s/d)_1$ hybrid states (4355 MeV) and charmonium $3p$ states (4369 MeV).

(ix) $Y(4320)$, $Y(4360)$, and $Y(4390)$ [18,41,42] are compatible with our spin zero 1^{--} hybrid $2(s/d)_1$ (H_1') state (4366 MeV). Spin symmetry would in principle favor the latter, as it is observed in the $\pi^+\pi^- h_c$ channel rather than in the $\pi^+\pi^- J/\psi$ channel. However, the large mixing with a spin 1 charmonium (see Table IV and Fig. 8) makes the two first ones also acceptable. The absence of any other state in this region in Table IV leaves two of them with no assignment. They may be affected by the $D_0^*\bar{D}^*$ threshold (4407 MeV).

(x) $X(4500)$ [39] is compatible with our 0^{++} hybrid $1p_0$ (H_3) state (4566 MeV). However, it mixes very little with the spin 1 charmonium (see Table VI and Fig. 9), which does not help us to understand the observation in the $J/\psi\phi$ channel. It may be affected by the $D(2550)\bar{D}^*$ threshold (4557 MeV).

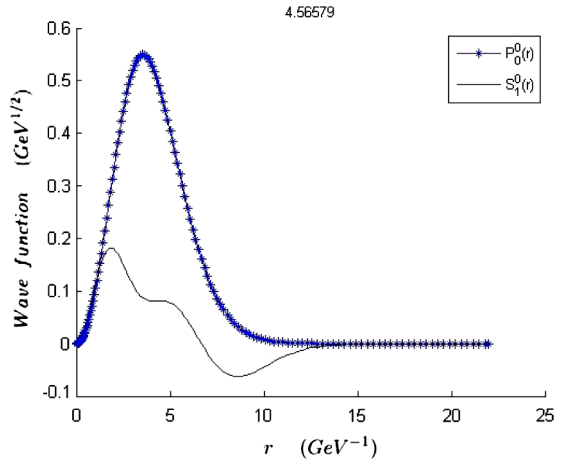

FIG. 9. The wave function of the charmonium 0^{++} $1p_0$ state.

(xi) $Y(4630)$ [18] is compatible with our 1^{--} charmonium $3d$ state (4559 MeV). It may be affected by the $D_{s1}\bar{D}_s^*$ thresholds (4572 and 4648 MeV).

(xii) $Y(4660)$ [18] is compatible with our spin zero 1^{--} hybrid $3(s/d)_1$ (H_1'') state (4711 MeV). The mixing with the spin 1 charmonium (see Table IV and Fig. 10) may explain the observed decays to vector charmonium. It may be affected by the $D_{s1}\bar{D}_s^*$ and $D_{s2}^*\bar{D}_s{}^*$ thresholds (4648 and 4685 MeV).

(xiii) $X(4700)$ [39] is compatible with our 0^{++} charmonium $4p$ state (4703 MeV).

The assignments above can be visualized in Fig. 11.

B. Bottom

(i) $\Upsilon(10\,860)$ [18,43] is compatible with our 1^{--} bottomonium $5s$ state (10 881 MeV). Upon mixing, it becomes lighter than the spin zero $2(s/d)_1$ hybrid nearby (see Table XIII and Fig. 12). Mixing may also explain the large spin symmetry violating decays to $\pi^+\pi^- h_b$ [44].

(ii) $Y_b(10\,890)$ [45] is compatible with our spin zero 1^{--} hybrid $2(s/d)_1$ state (10 890 MeV). Upon mixing, it becomes heavier than the $5s$ bottomonium nearby (see Table XIII and Fig. 13).

(iii) $\Upsilon(11\,020)$ [18,43] is about 1σ heavier than our 1^{--} bottomonium $4d$ state (10 942 MeV). It may be affected by the $B_1\bar{B}$ threshold (11 000 MeV).

VII. DISCUSSION

We have compared our results to other QCD-based approaches in Sec. V. We find good agreement with

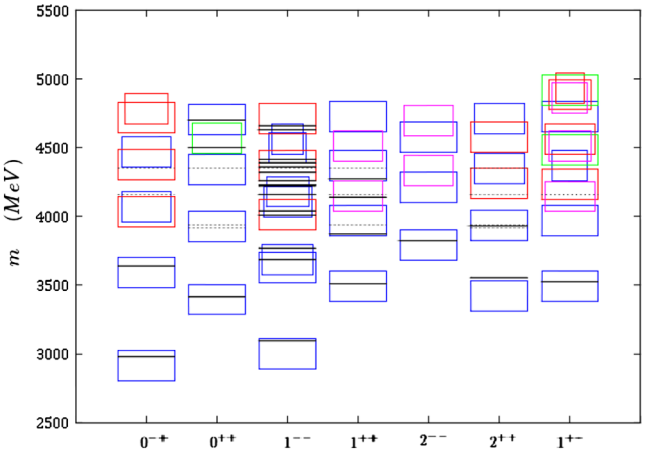

FIG. 11. Charmonium spectrum including hybrids. The height of the boxes corresponds to the error estimated at the end of Sec. IV C. Blue boxes correspond to a quarkonium, red boxes correspond to $(s/d)_1$ and $(p/f)_2$ hybrids, cyan boxes correspond to p_1 and d_2 hybrids, and green boxes correspond to p_0 hybrids. The black lines are experimental resonances assigned according to the discussion in Sec. VI. Solid (dashed) lines are resonances with a single (multiple) possible assignment(s). The widths of the boxes are chosen arbitrarily in order to facilitate identifications.

Born-Oppenheimer approaches that have appeared recently in the literature [9,10], as expected. However, the agreement with QCD sum rules and lattice QCD calculations is marginal. The lattice calculations in anisotropic lattices and unphysical quark masses tend to give a heavier hybrid spectrum, both in relativistic implementations of heavy quarks [34,36] as well as in lattice NRQCD [4]. Nevertheless, in Ref. [35], a lattice calculation in which both the continuum and the chiral extrapolations are carried out, the three states found that are not identified with known quarkonia fit well in our spectrum. In particular,

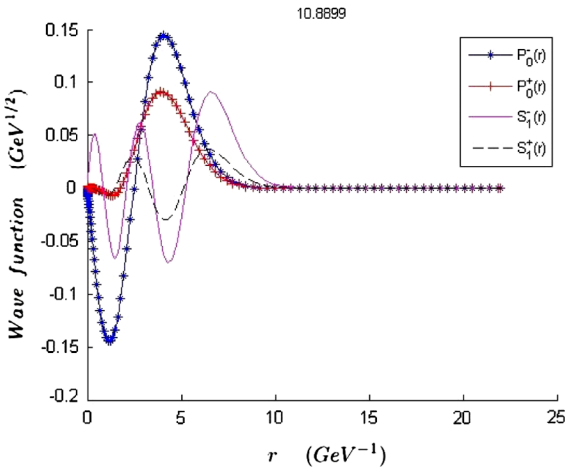

FIG. 12. The wave function of the bottomonium 1^{--} $5s$ state.

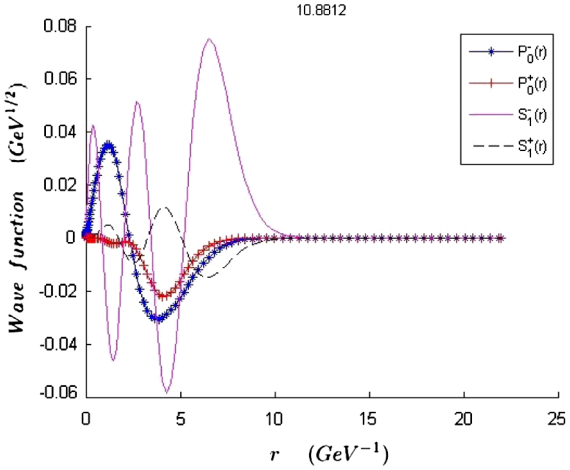

FIG. 13. The wave function of the bottomonium 1^{--} $2(s/d)_1$ state.

the 1^{--} state is compatible with the one in our lightest hybrid multiplet.

It is remarkable that the gross features of the experimental charmonium and bottomonium spectrum, including isospin zero XYZ states, can be understood from our results. The main improvement with respect to previous works is that, in addition to the Cornell potential for the quarkonium sector and the Born-Oppenheimer potentials for the hybrid sector, we include the leading mixing term between those sectors. The mixing term implies that the actual physical states are a superposition of spin zero (1) hybrids and spin 1 (zero) quarkonium. This facilitates the identification of certain Y states as hybrids, since otherwise the apparent spin symmetry violating decays were difficult to understand [10]. We would like to emphasize that the mixing term we use is essentially derived from NRQCD, and hence from QCD. Its short and long distance behaviors are obtained in a model-independent way. The model dependence comes in through the interpolation we use. We have chosen the sign combination and a value of the free parameter such that a large mixing is favored. It would be very important to have a lattice evaluation of the mixing potential to validate these choices (or otherwise). We have produced formulas (28) that can be easily implemented on the lattice (see for instance Refs. [29,46]).

There appear to be too many known isospin zero 1^{--} charmonium resonances to fit our spectrum in Table IV (see also Fig. 11). If we assign the $Y(4008)$ to the $1(s/d)_1$ state, then $\psi(4040)$ and $\psi(4160)$ naturally fall into the $3s$ and $2d$ states respectively. However, the $X(4230)/Y(4220)$ are also candidates for the $2d$ state. A possible way out would be to disregard $Y(4008)$, as it is a very wide resonance that has only been observed by Belle. Then, $\psi(4040)$ would be assigned to the $1(s/d)_1$ state, $\psi(4160)$ to the $3s$ state, and $X(4230)/Y(4220)$ to the $2d$ state. The

fact that the $1(s/d)_1$ state has about a 30% quarkonium component according to the seventh column of Table IV (see also Fig. 6) may explain why it has been labeled as $\psi(4040)$. For the next state, $2(s/d)_1$, there are three competing resonances $Y(4320)$, $Y(4360)$, and $Y(4390)$. This makes us suspect that they could correspond to the same state. Indeed, the decay widths of $Y(4320)$ and $Y(4360)$ are compatible and the one of $Y(4390)$ is less than 1σ away. Concerning the masses, $Y(4320)$ and $Y(4360)$ are less than 1σ away, but $Y(4390)$ is more than 5σ away, which casts some doubts on the suggested identification. Leaving this puzzle aside, there would only be one state to be discovered below the $Y(4660)$, the $3d$ around 4560 MeV.

If we assume for the $2(s/d)_1$ states the mixing displayed in column 7 of Table IV and the decay width in Table III for the hybrid component, we obtain

$$\Gamma(Y(4320/4360/4390) \to h_c + \text{l.h.}) = 14(12)\ \text{MeV}, \tag{55}$$

where l.h. stands for light hadrons. Analogously, for the $X(4230)/Y(4220)$ state, we have

$$\Gamma(X(4230)/Y(4220) \to h_c + \text{l. h.}) = 17(15)\ \text{MeV}. \tag{56}$$

Concerning the 1^{--} bottomonium resonances, all of them fit in our spectrum in Table XIII. In addition, there should be three states still to be discovered below the $\Upsilon(10860)$, the $2d$, $1(s/d)_1$, and $3d$ around 10 440, 10 690, and 10 710 MeV respectively.

If we take the mixing in column 5 of Table XIII and the decay width in Table III for the hybrid component, we can also estimate the following decay widths for the bottomonium:

$$\begin{aligned}\Gamma(\Upsilon(10\,860) \to h_b + \text{l.h.}) &= 3(1)\ \text{MeV}\\ \Gamma(Y_b(10\,890) \to h_b + \text{l.h.}) &= 13(6)\ \text{MeV}.\end{aligned} \tag{57}$$

According to our identifications in Sec. VI, we can infer the quantum numbers of some XYZ states:

(i) $X(3915)$ should be the χ'_{c0} (0^{++}).
(ii) $X(3940)$ should be the h'_c (1^{+-}).

It is important to keep in mind that there are further $1/m_Q$ corrections to the hybrid spectrum beyond those that induce mixing between hybrids and quarkonia we have focused on. In particular, the fine and hyperfine splittings of hybrids may appear at $\mathcal{O}(1/m_Q)$ rather than at $\mathcal{O}(1/m_Q^2)$, as those of the quarkonium. Indeed, the following terms are compatible with the symmetries of (3),

$$i\epsilon^{ijk} V^S(r)\, tr(H^{i\dagger}[\sigma^k, H^j]), \tag{58}$$

$$i\epsilon^{ijk} V^L(r)\, tr(H^{i\dagger} L^k H^j) \tag{59}$$

(L^k is the angular momentum operator), and may appear at $\mathcal{O}(1/m_Q)$ in the matching to NRQCD.

Before closing, let us briefly discuss the important question of how the lattice potentials we use (Fig. 1) may change in the case $n_f = 3$ (three light quarks). We know that Σ_g^+ does not change much, and this is also so for Π_u [47], at least up to moderately large distances. Nothing is known about Σ_u^-, but there is no reason to expect a different behavior. Two major qualitative features arise, though. The first one is the appearance of heavy-light meson pairs, which amount to roughly horizontal lines at the threshold energies in Fig. 1. These states interact with the remaining potentials already at leading order and may in principle produce important distortions with respect to the $n_f = 0$ case. In practice, we only know how they cross-talk to the Σ_g^+ state and turn out to produce a tiny disturbance to the spectrum, apart from avoiding level crossing [48]. Hence, we expect the effects of $n_f \neq 0$ to be important only when our states are very close to some heavy-light meson pair threshold. This is the reason why we quoted the location of nearby thresholds when identifying our hybrid candidates with XYZ states in Sec. VI. The second one is the appearance of light quark excitations, in addition to the gluon ones, in the static spectrum of Fig. 1. They may have different quantum numbers, for instance nonzero isospin (in this case, they may be relevant to the experimentally discovered charged Z states). We do not know anything about those, and as pointed out in Ref. [49] and more recently emphasized in Refs. [9,50], it would be extremely important to have lattice QCD evaluations of the static energies of light quark excitations. We suspect that light quark excitations with the same quantum numbers as the gluonic ones will only provide small modifications to the hybrid potentials, since they correspond to higher-dimensional operators. In this respect, it is significant that tetraquark models also have difficulties in encompassing the $X(4140)$ in their spectrum together with $X(4237)$, $X(4500)$, and $X(4700)$ [51]. In fact, the $X(4140)$ structure may be due to a threshold enhancement according to some authors [52–54]. This means that tetraquarks with the same quantum numbers as hybrids will in general be hidden in the spectrum of the latter.

VIII. CONCLUSIONS

We have calculated the charmonium and bottomonium hybrid spectrum in a QCD-based approach, including for the first time the mixing with standard charmonium and bottomonium states. The latter leads to enhanced spin symmetry violations, which are instrumental in identifying a number of XYZ states as hybrid states. Most of the isospin zero XYZ states fit well in our spectrum, either as hybrids or as standard quarkonium states. We have also estimated several decay widths.

ACKNOWLEDGMENTS

J. S. thanks Josep Taron for collaboration in the early stages of this work, Jaume Tarrús for discussions, and Antonio Pineda for clarifications on Ref. [16]. We have been supported by the Spanish Excellence Network on Hadronic Physics Grant No. FIS2014-57026-REDT. J. S. also acknowledges support from the 2014-SGR-104 grant (Catalonia); Projects No. FPA2013-4657, No. FPA2013-43425-P, No. FPA2016-81114-P, and No. FPA2016-76005-C2-1-P (Spain).

APPENDIX A: QUARKONIUM

A conventional quarkonium, namely, $Q\bar{Q}$ in a color singlet state, can be described by the Schrödinger equation using the ground state potential $V_{\Sigma_g^+}(r)$,

$$h = -\frac{\mathbf{\nabla}^2}{m_Q} + V_{\Sigma_g^+}(r). \tag{A1}$$

We approximate $V_{\Sigma_g^+}(r)$ by the Cornell potential,

$$V_{\Sigma_g^+}(r) \approx -\frac{k_g}{r} + \sigma_g r + E_g^{Q\bar{Q}}, \tag{A2}$$

where we take

$$k_g = 0.489, \qquad \sigma_g = 0.187\ \text{GeV}^2, \tag{A3}$$

which describes lattice data well; see Fig. 2. $E_g^{Q\bar{Q}}$ will be tuned independently for the charmonium and bottomonium. We write the wave function as $S(\mathbf{r}) = \frac{R_L(r)}{r} Y_{LM}(\theta,\phi)$, which leads to the reduced equation:

$$\left(-\frac{1}{m_Q}\frac{\partial^2}{\partial r^2} + \frac{L(L+1)}{m_Q r^2} + V_{\Sigma_g^+}(r)\right) R_L(r) = E R_L(r). \tag{A4}$$

The different eigenvalues of this equation correspond to the energy levels of a heavy quarkonium, many of which have been experimentally confirmed for the charmonium and bottomonium [18]. We fix $E_g^{Q\bar{Q}}$ by making the charmonium and bottomonium spectrum to best agree with the respective experimental spin averages. We obtain

$$E_g^{c\bar{c}} = -0.242\ \text{GeV}, \qquad E_g^{b\bar{b}} = -0.228\ \text{GeV}. \tag{A5}$$

Table V shows the results in terms of $M_{Q\bar{Q}} = 2m_Q + E$ for $Q = c, b$ of Eq. (A4) for the lower nL energy states. It also shows the expectation value of the momentum, the inverse radius, the expected size of the higher order corrections, and our error estimate. $V^{(1)}$, $V^{(2)}_{vd}$ (velocity dependent), and $V^{(2)}_{vi}$ (velocity independent) depend on $\Lambda_{\rm QCD}$ and r. We take $\Lambda_{\rm QCD} = 400$ MeV and estimate them as follows. If $\Lambda_{\rm QCD} > 1/\langle r\rangle$, we take them as $\Lambda^2_{\rm QCD}$, $\Lambda_{\rm QCD}\langle p\rangle^2$, and $\Lambda^3_{\rm QCD}$ respectively. If $\Lambda_{\rm QCD} < 1/\langle r\rangle$, we take them according to the weak coupling scalings $\alpha_s^2/\langle r\rangle^2$, $\alpha_s\langle p\rangle^2/\langle r\rangle$, and $\alpha_s/\langle r\rangle^3$ respectively, where α_s is the one-loop running coupling constant evaluated at the scale $1/\langle r\rangle$. The total error is obtained by summing in quadrature these estimates and the relativistic correction to the kinetic energy displayed in the eighth column. We observe that the errors for the charmonium are rather large and are dominated by the velocity-dependent potential. We also display the experimental results in the last column.

TABLE V. Masses, average momentum, inverse radii, expected sizes of higher order contributions ($1/m_Q$ potential, $1/m_Q^2$ velocity-dependent potential, $1/m_Q^2$ velocity-independent potentials, $1/m_Q^3$ kinetic energy), and estimated errors (in MeV) for the charmonium (upper) and bottomonium (lower). The error is estimated by summing in quadrature the expected sizes of the higher order contributions (see the text for details on the latter). We have taken $m_c = 1.47$ GeV and $m_b = 4.88$ GeV. The experimental numbers are displayed in the last column.

nL	$M_{Q\bar{Q}}$	$\langle p\rangle$	$\frac{1}{\langle r\rangle}$	$\frac{V^{(1)}}{m_Q}$	$\frac{V^{(2)}_{vd}}{m_Q^2}$	$\frac{V^{(2)}_{vi}}{m_Q^2}$	$\frac{p^4}{8m_Q^3}$	$\Delta M_{Q\bar{Q}}$	$E_{\rm exp}$
$1s$	3068	738	518	54	71	35	12	96	3068
$2s$	3678	836	259	109	129	30	19	173	3674
$3s$	4130	935	186	109	162	30	30	199	4039
$4s$	4517	1019	149	109	192	30	42	227	4421
$5s$	4865	1097	127	109	223	30	57	256	?
$1p$	3494	753	317	109	105	30	13	155	3525
$2p$	3968	871	209	109	140	30	23	182	3927
$3p$	4369	966	162	109	173	30	34	209	?
$4p$	4726	1048	135	109	203	30	47	237	?
$5p$	5055	1136	119	109	239	30	66	272	?
$1s$	9442	1546	1028	29	37	17	6	50	9445
$2s$	10 009	1408	432	14	22	2	4	26	10 017
$3s$	10 356	1494	295	33	38	3	5	50	10 355
$4s$	10 638	1594	232	33	43	3	7	54	10 579
$5s$	10 885	1692	195	33	48	3	9	59	10 876
$1p$	9908	1268	531	17	19	3	3	26	9900
$2p$	10 265	1386	332	33	32	3	4	46	10 260
$3p$	10 553	1504	252	33	38	3	5	51	?
$4p$	10 806	1612	207	33	44	3	7	55	?
$5p$	11 035	1727	180	33	50	3	10	61	?

APPENDIX B: EXTRACTION OF $g\Lambda'$ AND $g\Lambda'''$ FROM LATTICE DATA

$g\Lambda'$ and $g\Lambda'''$ also appear in the $1/m_Q^2$ quarkonium potentials [26,28]. Following the notation of Ref. [30], we

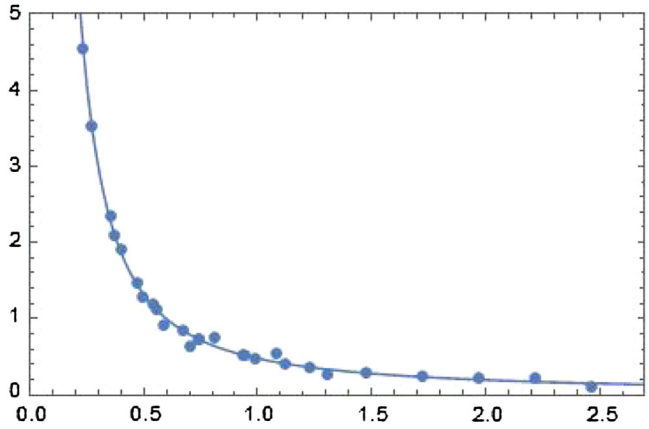

FIG. 14. $V_2'(r)$ in units of r_o^{-2} against r units of r_o, $r_o \sim 0.5$ fm.

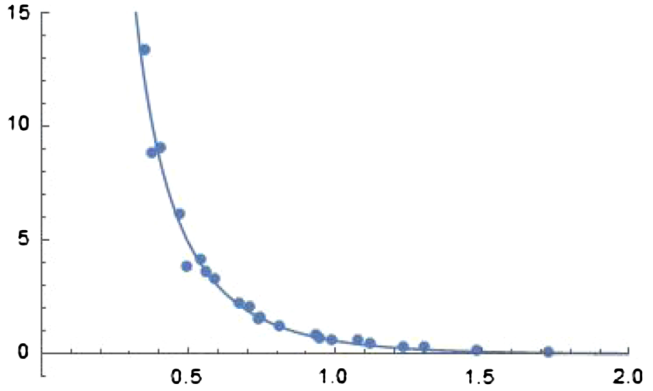

FIG. 15. $V_3(r)$ in units of r_o^{-3} against r in units of r_o, $r_o \sim 0.5$ fm.

have that the long distance behavior of the spin-orbit, tensor, and spin-spin potentials reads

$$V_2'(r) = 2rV_{\mathbf{L}_2\mathbf{S}_1}^{(1,1)} = -\frac{2c_F g^2\Lambda^2\Lambda'}{\kappa r} = -\frac{2c_F g\Lambda'}{r}$$
$$V_3(r) = 12V_{\mathbf{S}_{12}}^{(1,1)} = \frac{2\pi^3 c_F^2 g^2 \Lambda'''^2}{15\kappa^2 r^5}$$
$$V_4(r) = 3V_{\mathbf{S}^2}^{(1,1)} = \frac{\pi^3 c_F^2 g^2 \Lambda'''^2}{30\kappa^2 r^5}. \tag{B1}$$

We shall take the tree level value for c_F, $c_F = 1$.

For the spin-orbit potential, a simple interpolation of the expected long and short distance behavior, namely,

$$V_2'(r) = \frac{A}{r^2} + \frac{B}{r}, \tag{B2}$$

already produces a good fit to data ($R^2 = 0.998$; see Fig. 14). We obtain $A = 0.181$ and $B = 0.295$ in units of r_0, which translates to $|g\Lambda'| = 0.059$ GeV. If we restrict ourselves to the longer distance points (from seven to three) and fit the expected long distance behavior only, we obtain worse fits ($R^2 \lesssim 0.977$) with numbers about 40% higher, which may serve to estimate the error.

For the tensor potential, the following interpolation, which also has the right short and long distance behaviors, produces a good fit to data ($R^2 = 0.996$; see Fig. 15):

$$V_3(r) = \frac{C + Dr}{r^3 + r^6}. \tag{B3}$$

We obtain $C = 0.191$ and $D = 1.00$ in units of r_0, which translates to $|g\Lambda'''| = 0.230$ GeV. We have checked that if we restrict ourselves to the longer distance points (from seven to three) and fit the expected long distance behavior only, we obtain numbers compatible with the latter within a 35% error. $|g\Lambda'''|$ may also be obtained from the long distance behavior of the spin-spin potential. However, we have not been able to find a good fit to the data of Ref. [30], neither using simple interpolations between the expected short and long distance behavior nor to the expected long distance behavior for the longer distance points (from nine to three).

APPENDIX C: TENSOR SPHERICAL HARMONICS

We follow the notation of Ref. [15]. We define

$$Y_{\mathcal{J}M}^{ijLJ} = \sum_{\nu=0,\pm1} C(J1\mathcal{J}; \mathcal{M} - \nu\nu) Y_{J\mathcal{M}-\nu}^{iL} \chi_\nu^j, \tag{C1}$$

where Y_{JM}^{iL} are the vector spherical harmonics,

$$Y_{JM}^{iL} = \sum_{\mu=0,\pm1} C(L1J; M - \mu\mu) Y_L^{M-\mu} \chi_\mu^i, \tag{C2}$$

where Y_L^M are the usual spherical harmonics and

$$\chi_{\pm1} = \mp \frac{1}{\sqrt{2}} \begin{pmatrix} 1 \\ \pm i \\ 0 \end{pmatrix}, \qquad \chi_0 = \begin{pmatrix} 0 \\ 0 \\ 1 \end{pmatrix}. \tag{C3}$$

$C(J_1 J_2 J; M_1 M_2)$ are the Clebsch-Gordan coefficients.

APPENDIX D: SPECTRUM

We display in this Appendix the tables for the full charmonium and bottomonium spectrum up to $\mathcal{J} = 2$, which includes hybrids and quarkonia states, except for the charmonium 1^{--} case that is displayed in Table IV.

TABLE VI. Spectrum of charmonium ($S = 1$) and hybrids ($S = 0$): 0^{++} states. Masses are in GeV. The % columns show the fraction of the hybrid components for the mass states in the previous column. The mixing potentials are fixed to $V_S^{\Pi}[+-]$ and $V_S^{\Sigma}[++]$. $m_c = 1.47$ GeV.

NL_J	$\lambda = 0$	%	$\lambda = 0.6$	%
$1p$	3.494	0	3.396	7
$2p$	3.968	0	3.925	1
$3p$	4.369	0	4.338	0
$1p_0$	4.486	100	4.566	98
$4p$	4.727	0	4.703	9
$2p_0$	4.920	100	4.965	94
$5p$	5.055	0	5.034	1

TABLE VII. Same as in Table VI for 1^{++} states.

NL_J	$\lambda = 0$	%	$\lambda = 0.6$	%
$1p$	3.494	0	3.492	0
$2p$	3.968	0	3.967	0
$1p_1$	4.145	100	4.146	100
$3p$	4.369	0	4.368	0
$2p_1$	4.511	100	4.512	100
$4p$	4.727	0	4.726	0
$3p_1$	4.863	100	4.863	99
$5p$	5.055	0	5.055	1

TABLE VIII. Same as in Table VI for 2^{++} states.

NL_J	$\lambda = 0$	%	$\lambda = 0.6$	%
$1p$	3.494	0	3.424	5
$2p$	3.968	0	3.937	7
$1f$	4.047	0	3.981	11
$1(p/f)_2$	4.231	100	4.240	81
$3p$	4.369	0	4.350	0
$2f$	4.428	0	4.391	77
$2(p/f)_2$	4.563	100	4.579	53
$4p$	4.727	0	4.709	3
$3f$	4.775	0	4.752	11
$3(p/f)_2$	4.886	100	4.909	78
$4(p/f)_2$	4923	100	4.952	94
$5p$	5.055	0	5.040	4

TABLE IX. Same as in Table VI for 2^{--} states.

NL_J	$\lambda = 0$	%	$\lambda = 0.6$	%
$1d$	3.793	0	3.792	0
$2d$	4.210	0	4.209	1
$1d_2$	4.334	100	4.335	100
$3d$	4.579	0	4.578	0
$2d_2$	4.693	100	4.694	99
$4d$	4.916	0	4.915	0
$3d_2$	5.036	100	5.037	100

TABLE X. Spectrum of charmonium ($S = 0$) and charmonium hybrids ($S = 1$): 0^{-+} states. Masses are in GeV. The % columns show the fraction of the hybrid components for the mass states in the previous column. The mixing potentials are fixed to $V_S^{\Pi}[+-]$ and $V_S^{\Sigma}[++]$. $m_c = 1.47$ GeV.

NL_J	$\lambda = 0$	%	$\lambda = 0.6$	%
$1s$	3.068	0	2.913	7
$2s$	3.678	0	3.591	8
$1(s/d)_1$	4.011	100	4.033	99
$3s$	4.131	0	4.069	1
$2(s/d)_1$	4.355	100	4.375	92
$4s$	4.512	0	4.468	7
$3(s/d)_1$	4.692	100	4.719	99
$4(s/d)_1$	4.718	100	4.781	96
$5s$	4.865	0	4.823	0
$5(s/d)_1$	5.043	100	5.055	96

TABLE XI. Same as in Table X for 1^{+-} states.

NL_J	$\lambda = 0$	%	$\lambda = 0.6$	%
$1p$	3.494	0	3.333	9
$2p$	3.968	0	3.901	2
$1p_1$	4145	100	4.146	100
$1(p/f)_2$	4231	100	4.242	99
$3p$	4.369	0	4.320	1
$1p_0$	4.486	100	4.511	98
$2p_1$	4.511	100	4.526	100
$2(p/f)_2$	4563	100	4.590	95
$4p$	4.727	0	4.686	8
$3p_1$	4863	100	4.863	100
$3(p/f)_2$	4886	100	4.901	99
$2p_0$	4920	100	4.936	95
$4(p/f)_2$	4923	100	4.959	100
$5p$	5.055	0	5.020	7

TABLE XII. Same as in Table X for 2^{-+} states.

NL_J	$\lambda = 0$	%	$\lambda = 0.6$	%
$1d$	3.793	0	3.721	6
$1(s/d)_1$	4.011	100	4.014	75
$2d$	4.210	0	4.199	80
$1d_2$	4334	100	4.335	100
$2(s/d)_1$	4.355	100	4.353	73
$1(d/g)_3$	4.435	100	4.443	100
$3d$	4.579	0	4.571	11
$3(s/d)_1$	4.692	100	4.690	97
$2d_2$	4.693	100	4.694	98
$4(s/d)_1$	4.718	100	4.713	96
$2(d/g)_3$	4.763	100	4.774	90
$4d$	4.916	0	4.911	27
$3d_2$	5.036	100	5.037	95
$5(s/d)_1$	5.043	100	5.084	98

TABLE XIII. Spectrum of bottomonium ($S=1$) and hybrids ($S=0$): 1^{--} states. Masses are in GeV. The % columns show the fraction of the hybrid components for the mass states in the previous column. The mixing potentials are fixed to $V_S^{\Pi}[+-]$ and $V_S^{\Sigma}[++]$. $m_b = 4.88$ GeV.

NL_J	$\lambda=0$	%	$\lambda=0.6$	%
$1s$	9.442	0	9.441	0
$2s$	10.009	0	10.000	2
$1d$	10.155	0	10.133	2
$3s$	10.356	0	10.352	0
$2d$	10.454	0	10.440	2
$4s$	10.638	0	10.635	1
$1(s/d)_1$	10.690	100	10.688	79
$3d$	10.712	0	10.713	56
$2(s/d)_1$	10.885	100	10.881	17
$5s$	10.886	0	10.890	75
$4d$	10.947	0	10.942	11
$3(s/d)_1$	11.084	100	11.086	98

TABLE XIV. Same as in Table XIII for 0^{++} states.

NL_J	$\lambda=0$	%	$\lambda=0.6$	%
$1p$	9.908	0	9.907	0
$2p$	10.265	0	10.264	0
$3p$	10.553	0	10.553	0
$4p$	10.806	0	10.805	0
$1p_0$	11.011	100	11.013	99

TABLE XV. Same as in Table XIII for 1^{++} states.

NL_J	$\lambda=0$	%	$\lambda=0.6$	%
$1p$	9.908	0	9.908	0
$2p$	10.265	0	10.265	0
$3p$	10.553	0	10.553	0
$1p_1$	10.761	100	10.761	99
$1p$	10.806	0	10.806	0
$2p_1$	10.970	100	10.970	99
$5p$	11.034	0	11.035	0

TABLE XVI. Same as in Table XIII for 2^{++} states.

NL_J	$\lambda=0$	%	$\lambda=0.6$	%
$1p$	9.908	0	9.898	1
$2p$	10.265	0	10.258	1
$1f$	10.348	0	10.331	2
$3p$	10.553	0	10.549	0
$2f$	10.615	0	10.603	5
$4p$	10.806	0	10.801	13
$1(p/f)_2$	10.819	100	10.820	91
$3f$	10.855	0	10.851	32
$2(p/f)_2$	11.005	100	11.009	80

TABLE XVII. Same as in Table XIII for 2^{--} states.

NL_J	$\lambda=0$	%	$\lambda=0.6$	%
$1d$	10.155	0	10.155	0
$2d$	10.453	0	10.454	0
$3d$	10.712	0	10.713	0
$1d_2$	10.870	100	10.870	100
$4d$	10.947	0	10.947	0
$2d_2$	11.074	100	10.074	100

TABLE XVIII. Spectrum of bottomonium ($S=0$) and bottomonium hybrids ($S=1$): 0^{-+} states. Masses are in GeV. The % columns show the fraction of the hybrid components for the mass states in the previous column. The mixing potentials are fixed to $V_S^{\Pi}[+-]$ and $V_S^{\Sigma}[++]$. $m_b = 4.88$ GeV.

NL_J	$\lambda=0$	%	$\lambda=0.6$	%
$1s$	9.442	0	9.427	1
$2s$	10.009	0	9.987	3
$3s$	10.356	0	10.343	1
$4s$	10.638	0	10.629	3
$1(s/d)_1$	10.690	100	10.693	99
$5s$	10.886	0	10.877	16
$2(s/d)_1$	10.885	100	10.890	81
$3(s/d)_1$	11.084	100	11.086	95

TABLE XIX. Same as in Table XVIII for 1^{+-} states.

NL_J	$\lambda=0$	%	$\lambda=0.6$	%
$1p$	9.908	0	9.886	2
$2p$	10.265	0	10.249	2
$3p$	10.553	0	10.543	0
$1p_1$	10.761	100	10.761	100
$4p$	10.806	0	10.798	1
$1(p/f)_2$	10.819	100	10.820	100
$2p_1$	10.970	100	10.969	100
$1p_0$	11.011	100	11.006	100

TABLE XX. Same as in Table XVIII for 2^{-+} states.

NL_J	$\lambda=0$	%	$\lambda=0.6$	%
$1d$	10.155	0	10.144	2
$2d$	10.454	0	10.444	3
$1(s/d)_1$	10.690	100	10.685	82
$3d$	10.712	0	10.717	52
$1d_2$	10.870	100	10.870	100
$2(s/d)_1$	10.885	100	10.886	94
$1(d/g)_1$	10.935	100	10.937	99
$4d$	10.947	0	10.945	13
$2d_2$	11.074	100	11.074	99

[1] S. L. Olsen, *Proc. Sci.*, Bormio2015 (2015) 050.
[2] W. E. Caswell and G. P. Lepage, Phys. Lett. **167B**, 437 (1986).
[3] G. T. Bodwin, E. Braaten, and G. P. Lepage, Phys. Rev. D **51**, 1125 (1995); **55**, 5853(E) (1997).
[4] K. J. Juge, J. Kuti, and C. J. Morningstar, Phys. Rev. Lett. **82**, 4400 (1999).
[5] G. Chiladze, A. F. Falk, and A. A. Petrov, Phys. Rev. D **58**, 034013 (1998).
[6] N. Brambilla, A. Pineda, J. Soto, and A. Vairo, Nucl. Phys. **B566**, 275 (2000).
[7] K. J. Juge, J. Kuti, and C. Morningstar, Phys. Rev. Lett. **90**, 161601 (2003).
[8] S. Perantonis and C. Michael, Nucl. Phys. **B347**, 854 (1990).
[9] E. Braaten, C. Langmack, and D. H. Smith, Phys. Rev. D **90**, 014044 (2014).
[10] M. Berwein, N. Brambilla, J. Tarrús Castellà, and A. Vairo, Phys. Rev. D **92**, 114019 (2015).
[11] R. Oncala and J. Soto, Eur. Phys. J. Web Conf. **137**, 06025 (2017).
[12] A. Pineda and J. Soto, Nucl. Phys. B, Proc. Suppl. **64**, 428 (1998).
[13] M. Luscher and P. Weisz, J. High Energy Phys. 07 (2002) 049.
[14] M. Luscher and P. Weisz, J. High Energy Phys. 07 (2004) 014.
[15] A. Galindo and P. Pascual, *Quantum Mechanics I* (Springer, Berlin, 1990), p. 334.
[16] G. S. Bali and A. Pineda, Phys. Rev. D **69**, 094001 (2004).
[17] R. Oncala, M.Sc. Thesis, Universitat de Barcelona, July 2016.
[18] C. Patrignani *et al.* (Particle Data Group), Chin. Phys. C **40**, 100001 (2016).
[19] N. Brambilla, A. Pineda, J. Soto, and A. Vairo, Rev. Mod. Phys. **77**, 1423 (2005).
[20] E. Braaten, C. Langmack, and D. H. Smith, Phys. Rev. Lett. **112**, 222001 (2014).
[21] N. Brambilla, A. Pineda, J. Soto, and A. Vairo, Phys. Rev. D **63**, 014023 (2000).
[22] A. Pineda and A. Vairo, Phys. Rev. D **63**, 054007 (2001); **64**, 039902(E) (2001).
[23] E. Eichten and F. Feinberg, Phys. Rev. D **23**, 2724 (1981).
[24] G. S. Bali, Phys. Rep. **343**, 1 (2001).
[25] N. Brambilla, D. Eiras, A. Pineda, J. Soto, and A. Vairo, Phys. Rev. D **67**, 034018 (2003).
[26] G. Perez-Nadal and J. Soto, Phys. Rev. D **79**, 114002 (2009).
[27] J. B. Kogut and G. Parisi, Phys. Rev. Lett. **47**, 1089 (1981).
[28] N. Brambilla, M. Groher, H. E. Martinez, and A. Vairo, Phys. Rev. D **90**, 114032 (2014).
[29] Y. Koma and M. Koma, Nucl. Phys. **B769**, 79 (2007).
[30] Y. Koma and M. Koma, *Proc. Sci.*, LAT2009 (2009) 122.
[31] L. Liu, G. Moir, M. Peardon, S. M. Ryan, C. E. Thomas, P. Vilaseca, J. J. Dudek, R. G. Edwards, B. Joó, and D. G. Richards (Hadron Spectrum Collaboration), J. High Energy Phys. 07 (2012) 126.
[32] A. Pineda, J. High Energy Phys. 06 (2001) 022.
[33] X. Liao and T. Manke, arXiv:hep-lat/0210030.
[34] G. K. C. Cheung, C. O'Hara, G. Moir, M. Peardon, S. M. Ryan, C. E. Thomas, and D. Tims (Hadron Spectrum Collaboration), J. High Energy Phys. 12 (2016) 089.
[35] K. Cichy, M. Kalinowski, and M. Wagner, Phys. Rev. D **94**, 094503 (2016).
[36] X. Liao and T. Manke, Phys. Rev. D **65**, 074508 (2002).
[37] W. Chen, R. T. Kleiv, T. G. Steele, B. Bulthuis, D. Harnett, J. Ho, T. Richards, and S. L. Zhu, J. High Energy Phys. 09 (2013) 019.
[38] Z. Q. Liu *et al.* (Belle Collaboration), Phys. Rev. Lett. **110**, 252002 (2013).
[39] R. Aaij *et al.* (LHCb Collaboration), Phys. Rev. Lett. **118**, 022003 (2017).
[40] R. E. Mitchell (BESIII Collaboration), *Proc. Sci.*, ICHEP2016, 600 (2016).
[41] M. Ablikim *et al.* (BESIII Collaboration), Phys. Rev. Lett. **118**, 092001 (2017).
[42] M. Ablikim *et al.* (BESIII Collaboration), Phys. Rev. Lett. **118**, 092002 (2017).
[43] D. Santel *et al.* (Belle Collaboration), Phys. Rev. D **93**, 011101 (2016).
[44] R. Mizuk *et al.* (Belle Collaboration), Phys. Rev. Lett. **117**, 142001 (2016).
[45] I. Adachi *et al.* (Belle Collaboration), Phys. Rev. D **82**, 091106 (2010).
[46] Y. Koma, M. Koma, and H. Wittig, Phys. Rev. Lett. **97**, 122003 (2006).
[47] B. Bolder, T. Struckmann, G. S. Bali, N. Eicker, T. Lippert, B. Orth, K. Schilling, and P. Ueberholz, Phys. Rev. D **63**, 074504 (2001).
[48] G. S. Bali, H. Neff, T. Düssel, T. Lippert, and K. Schilling (SESAM Collaboration), Phys. Rev. D **71**, 114513 (2005).
[49] N. Brambilla, A. Vairo, A. Polosa, and J. Soto, Nucl. Phys. B, Proc. Suppl. **185**, 107 (2008).
[50] E. Braaten, Phys. Rev. Lett. **111**, 162003 (2013).
[51] A. Esposito, A. Pilloni, and A. D. Polosa, Phys. Rep. **668**, 1 (2017).
[52] E. van Beveren and G. Rupp, arXiv:0906.2278.
[53] X. H. Liu, Phys. Lett. B **766**, 117 (2017).
[54] P. G. Ortega, J. Segovia, D. R. Entem, and F. Fernández, Phys. Rev. D **94**, 114018 (2016).